Marine and Petroleum Geology 134 (2021) 105343

Contents lists available at ScienceDirect

Marine and Petroleum Geology

journal homepage: www.elsevier.com/locate/marpetgeo

Upper Jurassic to Lower Cretaceous source rocks in the Norwegian Barents Sea, part II: Insights from open- and closed-system pyrolysis experiments

Andrés Cedeño [a,*], Sverre Ohm [a], Alejandro Escalona [a], Dora Marín [a], Snorre Olaussen [b], Thomas Demchuk [c]

[a] University of Stavanger, Norway
[b] The University Centre in Svalbard, Norway
[c] Louisiana State University, USA

ARTICLE INFO

Keywords:
Source rock
Petroleum generation potential
GC-Pyrolysis
Bulk kinetics
Compositional kinetics
Barents sea
Hekkingen formation

ABSTRACT

The petroleum generation potential of Upper Jurassic to Lower Cretaceous organic rich shales from the southwestern Barents Sea was evaluated using bulk and quantitative pyrolysis analysis. Fifteen thermally-immature samples from the Hekkingen Formation with differing organic facies, as defined by maceral composition, were subjected to total organic carbon, Rock-Eval pyrolysis, pyrolysis gas chromatography, bulk kinetics, and micro-scale sealed vessel pyrolysis analyses. The results were employed to characterize differences in source rock kerogens, gross petroleum type, and the compositional evolution of the generated fluids as well as their physical properties (i.e. gas to oil ratio, saturation pressure, and formation volume factor) as a function of increasing maturity.

The investigated samples contain varying proportions of kerogen type II and III. Heterogeneities in the kerogen composition result in different orders of thermal stability, with the onset of petroleum generation predicted to occur over a high and broad temperature range from 123 °C to 144 °C (at 3.3C°/Ma). Reduced kerogen stability associated with elevated sulfur contents is only documented in a few samples. Most of the analyzed samples have the potential to generate low GOR oils of an intermediate to aromatic, low wax paraffinic-naphthenic-aromatic (P–N-A) composition and variable amounts of wet gas. Petroleums of similar compositional and physical properties are predicted to have been generated from the natural maturation sequence of various organic facies in thermally mature areas of the Hammerfest Basin and the Ringvassøy-Loppa High and Bjørnøyrenna fault complexes. Vitrinite-rich sources in the Fingerdjupet Sub-basin and the Troms-Finnmark Fault Complex have potential for gas and condensate generation.

1. Introduction

The Norwegian Barents Sea hosts various petroleum source rock intervals ranging in age from Carboniferous to Early Cretaceous (Henriksen et al., 2011a; Ohm et al., 2008; Abay et al., 2017). The clastic rocks of the Upper Jurassic Hekkingen Formation constitute the most widespread and one of the most prolific sourcing intervals. These extended deposits are records of a Late Jurassic epicontinental sea inundating vast areas of the western Barents Shelf (Fig. 1). Development of suboxic to anoxic conditions and the coincidental increase in biological carbon productivity favored accumulation of organic-carbon-rich sediments. Total organic carbon (TOC) values in the Alge Member are typically higher than in the overlying Krill Member as demonstrated by Cedeño et al., 2021 and affirmed by the general literature (Henriksen et al., 2011a; Ohm et al., 2008; Abay et al., 2017).

Geochemical characterization of oils in the southwestern Barents Sea has been conducted by Ohm et al. (2008), Duran et al. (2013a), Killops et al. (2014), Murillo et al. (2016) and Lerch et al. (2016). Their studies concluded that the organic-rich facies of the Hekkingen Formation provides a source for some of the migrated petroleum within the Snøhvit and Goliath fields, and various sub-commercial accumulations across the southwestern Barents Sea. These observations are also supported by the basin modelling work of Duran et al. (2013a and b).

Cedeño et al., 2021 analyzed the geochemistry and compositions of the solid organic matter constituents of more than 300 samples widely distributed across the southwestern Barents Sea to characterize the

* Corresponding author.
E-mail address: andres.f.cedenomotta@uis.com (A. Cedeño).

https://doi.org/10.1016/j.marpetgeo.2021.105343
Received 9 April 2021; Received in revised form 31 August 2021; Accepted 22 September 2021
Available online 1 October 2021

Fig. 1. Paleogeographic location of the Barents Sea within the northwestern European Shelf at the Oxfordian-Kimmeridgian boundary (Paleomap Project, Scotese, 2016).

depositional nature and organic facies variability within the Hekkingen Formation. This study recognized remarkably high contents of oil-prone amorphinite in the southern part of Bjørnøyrenna Fault Complex as well as a westwards enrichment in marine algae within the Hammerfest Basin, the latter being more pronounced within the Alge Member (Fig. 2). Their study also showed that the Hekkingen Formation in the Nordkapp Basin and the adjacent Bjarmeland and eastern Finnmark platforms contains mostly terrestrial-derived particles.

The generative potential of source rock kerogens depends essentially on the character of the primary biomass and dictates the gross composition of generated petroleum (Demaison and Moore, 1980; di Primio and Horsfield, 2006). Inherently, varying proportions of marine and terrestrial macerals reported within the Hekkingen Formation invokes heterogeneity in kerogen thermal stability and, importantly, in physicochemical properties of the generated petroleum. In this study, non-isothermal open-system pyrolysis is used for modeling bulk kinetic parameters of primary petroleum generation from fifteen samples chosen to capture the variability in organic facies, as defined by maceral compositions, within the Hekkingen Formation. Results from open pyrolysis-gas chromatography (Py-GC) and compositional kinetic models are employed to predict petroleum type and physical properties under increasing maturity. Additionally, the present study produces a map that illustrates the variation in kinetic parameters and predicted petroleum types generated from the natural maturation series of various organic facies across the southwestern Barents Sea. The results of this study can be readily implemented in basin and petroleum system studies of the Barents Sea and other basins alike.

2. Structural setting and stratigraphy

The western Barents Sea is divided into several basins (Hammerfest, Tromsø, Bjørnøya, Nordkapp, Fingerdjupet), platforms (Bjarmeland and Finnmark), and structural highs (Loppa and Central highs and Samson and Svalis domes) separated by major fault complexes (Troms-Finnmark, Ringvassøy-Loppa, Asterias, Bjørnøyrenna, Nysleppen and Hoop) (Fig. 2; Clark et al., 2014; Blaich et al., 2017; Indrevær et al., 2017; Mulrooney et al., 2017; Serck et al., 2017; Kairanov et al., 2019; Faleide et al., 2019; Tsikalas et al., 2021). Long term Cenozoic uplift in the greater Barents Sea has resulted in net erosion values that vary from 0 to more than 3000 m (Riis, 1996; Doré et al., 2000; Cavanagh et al., 2006; Henriksen et al., 2011b).

The geological evolution and deposition of Middle Jurassic to Lower Cretaceous successions within the western Barents Sea was largely controlled by a global eustatic sea level rise and renewed tectonic activity (Sund et al., 1986; Berglund et al., 1986; Faleide et al., 1993; Gernigon et al., 2014; Serck et al., 2017; Rojo et al., 2019; Kairanov et al., 2021). Development of an epicontinental sea and intensified organic carbon productivity during the Late Jurassic allowed for deposition and burial of organic rich sediments over vast areas of the continental shelf. These clastic sediments are collectively referred to as the Hekkingen Formation (Norwegian Petroleum Directorate, https://www.npd.no/en/). This formation has an unconformable basal contact with rocks of the Fuglen Formation, although it may locally grade to a conformable surface, and unconformably underlies the Lower Cretaceous units along the regionally extended Base Cretaceous Unconformity (Århus, 1991; Bugge et al., 2002; Marín et al., 2018; Wierzbowski and Smelror, 2020).

The sedimentary character of the Hekkingen Formation changes from a black shale-dominated succession at the base to a silt-dominated succession at the top, and is, therefore, subdivided into the Alge and Krill members, respectively (Dalland et al., 1988; Mørk et al., 1999). Based on palynological data, Dalland et al. (1988), Georgiev et al. (2017), Mørk et al. (1999), and Smelror et al. (2001) estimate an Oxfordian to Kimmeridgian age for the lower Alge Member and a Kimmeridgian to Ryazanian age for the upper Krill Member.

The Alge Member ranges in thickness from 35 m in the Hammerfest Basin to up to 185m (well 7129/8-1-s) in the Bjørnøyrenna Fault Complex (Mørk et al., 1999; Marín et al., 2020; Cedeño et al., 2021). These black shales are largely associated with deposition in an oxygen-depleted shelf (Mørk et al., 1999), but short phases of more oxygenated bottom water conditions have also been recognized. The Krill Member displays higher variations in thickness, from absent in some wells in the southwestern Barents Sea (e.g. 7120/2-3s) to over 600 m within the Bjørnøyrenna Fault Complex (Marín et al., 2020). These sediments were deposited in a wide range of bathymetric conditions ranging from a shallow shelf to deep marine environments (Mørk et al., 1999; Marín et al., 2020; Helleren et al., 2020). Marín et al. (2020) interpret the Krill Member to have been deposited during a more tectonically active period.

Total organic carbon data shows that the main section of enhanced organic richness occurs within the lower Alge Member (Henriksen et al., 2011a, 2011b; Marín et al., 2020; Cedeño et al., 2021). Hydrogen indices (HI) from 50 to 430 mg hydrocarbon per gram TOC (50–430 mg HC/g TOC) are recorded for Alge and Krill immature samples, which are typically associated with kerogen assemblages ranging from III to II. This suggests that both the Alge Member and the more discrete organic-rich Krill Member possess similar generative potential (Ohm et al., 2008; Henriksen et al., 2011a, 2011b; Cedeño et al., 2021). HI values in the central-western Hammerfest Basin and the Bjørnøyrenna Fault Complex are low owning to high thermal maturity. Cedeño et al., 2021 estimate an original HI value of 400 and at least 500 mg HC/g TOC for the Hekkingen members in these areas, respectively, which are consistent with Type II kerogens.

3. Samples and methods

A total of 235 cuttings and core samples from the Hekkingen Formation were collected from 35 oil and stratigraphic (i.e. IKU stratigraphic Drilling Projects) wells distributed across the southwestern areas of the Barents Sea (Fig. 2). All samples were obtained from the Norwegian Petroleum Directorate (NPD) and SINTEF well repositories.

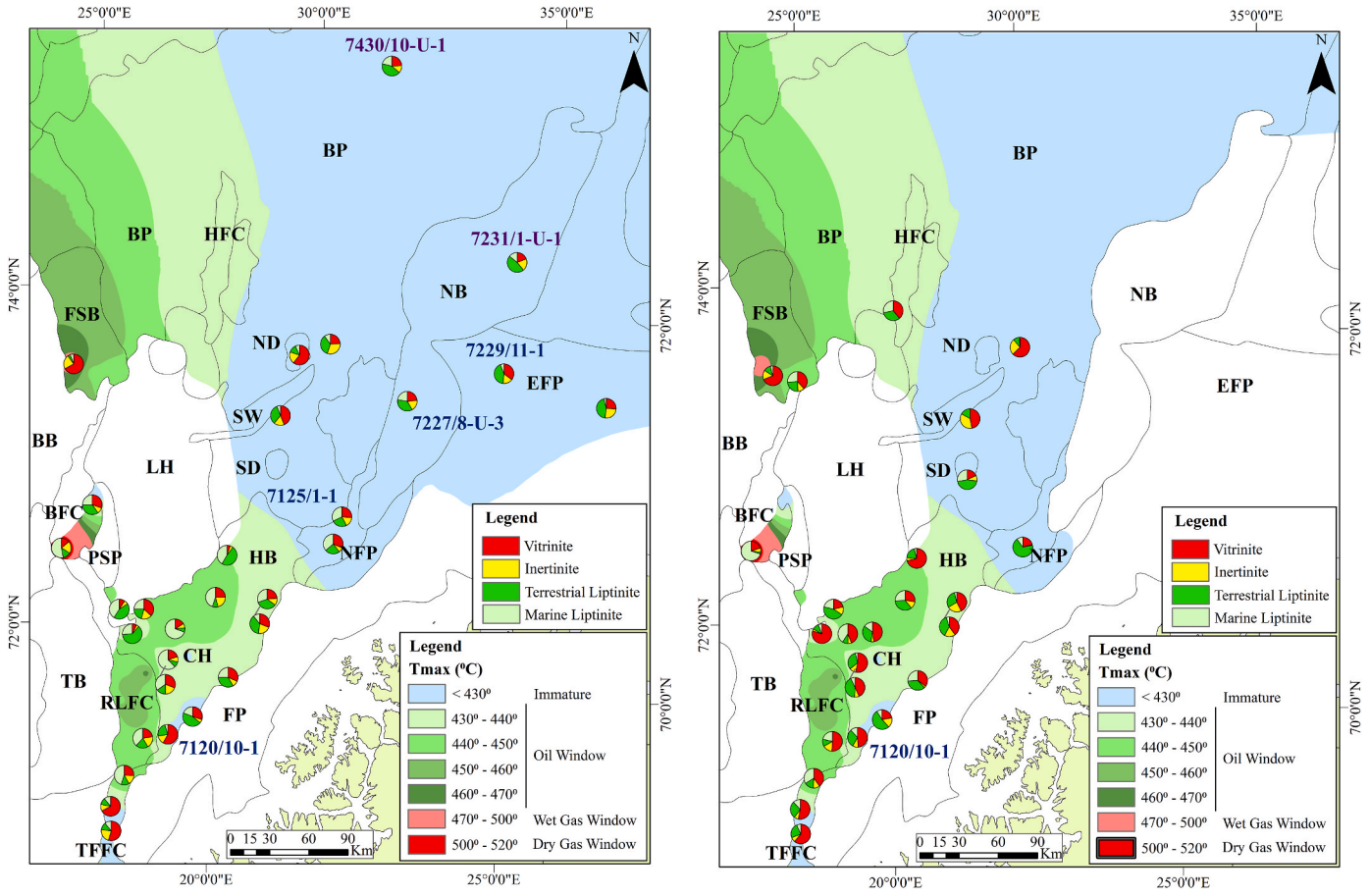

Fig. 2. Map of the southwestern Barents Sea illustrating the variability in maceral compositions within the Alge (**A**) and Krill (**B**) members across the various geological provinces. The pie diagrams represent the average (i.e. per well) maceral compositions calculated from the microscopic analysis in Cedeño et at. (2021). Relevant wells used in this study are shown (See Table 1). A present-day maturity overlay of the Hekkingen Formation calculated from Tmax Rock-Eval data is also displayed. BP= Bjarmeland Platform, HFC= Hoop Fault Complex. MB = Maud Basin, MH = Mercurius High, NB= Nordkapp Basin, EFP = eastern Finnmark Platform, ND= Norvarg Dome, SG= Swaen Graben, SD= Samson Dome, FSB= Fingerdjupet Sub-basin, BB= Bjørnøya Basin, BFC= Bjørnøya Fault Complex, PSP= Polhem Sub-platform, LH = Loppa High, NFC= Nysleppen Fault Complex, HB= Hammerfest Basin, CH= Central High, RLFC = Ringvassøy-Loppa Fault Complex, TB = Tromsø Basin, FP= Finnmark Platform, TFFC = Troms-Finnmark Fault Complex.

The sampled intervals were selected based on the stratigraphic boundaries of the Hekkingen Formation as defined by the NPD and preexisting geochemical results from well completion reports.

In an initial phase, samples underwent TOC and Rock-Eval analysis. Aliquots of each sample were pulverized and subdivided in two. The TOC content was quantified with a LECO SC-632 combustion oven tuned

Table 1
Sample information, whole rock and maceral composition, and bulk source rock geochemical results (i.e. Rock-Eval and TOC) of the fifteen studied samples. These samples were selected from a regional study documented in Cedeño et al., 2021.

ID	Well	Depth	Sample	Whole rock composition %						Maceral composition %				TOC	HI	Tmax
		m	type	Clay	Quarzt	Sulfides	Carbonates	Bitumen	Macerals	Mar. Lip	Terr. Lip	Inertinite	Vitrinite	%	mgHC/gTOC	ºC
A	7120/10-1	1455	Cuttings	23	56	6	0	7	6	2	33	9	55	5.4	226	426
B	7120/10-1	1467	Cuttings	46	25	12	1	11	6	9	25	11	55	6.2	171	422
C	7120/10-1	1482	Cuttings	51	11	8	1	16	12	41	19	6	35	6.7	243	426
D	7125/1-1	1355	Cuttings	57	14	13	0	9	8	0	53	8	39	8.3	313	425
E	7125/1-1	1368	Cuttings	75	14	5	0	5	1	0	20	5	76	2.2	115	432
F	7125/1-1	1380	Cuttings	45	15	7	0	10	23	52	0	15	33	15.5	304	423
G	7125/1-1	1392	Cuttings	44	11	11	0	7	26	8	49	21	21	16.5	313	423
H	7220/5-2	1441	Cuttings	53	33	6	0	5	4	66	14	4	17	2.4	378	425
I	7227/8-U-3	39.9	Core	55	10	8	1	8	18	23	54	10	13	18.6	192	403
J	7227/8-U-3	44.0	Core	59	14	3	0	4	20	0	61	22	17	15.8	248	406
K	7227/8-U-3	48.78	Core	46	9	8	2	12	24	70	21	6	3	21.1	258	408
L	7229/11-1	1260	Cuttings	44	28	5	0	6	17	0	42	19	40	12.6	282	424
M	7231/1-U-1	65.5	Core	63	5	2	1	10	19	35	58	0	6	12.2	230	414
N	7430/10-U-1	44.1	Core	51	9	3	4	15	18	53	47	0	0	23.0	353	420
O	7430/10-U-1	46.95	Core	44	9	5	3	10	29	0	73	27	0	16.3	306	416

to an IR-detector. Rock-Eval pyrolysis was performed using a Rock-Eval 6 instrument, allowing direct measurement of free hydrocarbons (S_1), remaining hydrocarbon generative potential (S_2), carbon dioxide (CO_2) content produced during thermal cracking (S_3), and temperature of S_2 maxima (T_{max}) (Espitalié et al., 1977). All samples were also subjected to organic and mineral petrographic analysis following the methods described in Cedeño et al., 2021. Fifteen thermally-immature source rocks samples representing the most common maceral assemblages were selected for artificial maturation experiments (Table 1). To ensure thermal immaturity, sample selection was limited to wells drilled near structural highs (i.e. wells 7231-1-U-1, 7227/8-U-3, 7125/1-1) or well sections interpreted to have experienced significant organic matter dilution (i.e. well 7120/10–1; see Fig. 4 in Cedeño et al., 2021). Where available, core material was prioritized over cuttings.

Open-system pyrolysis-gas chromatography (Py-GC) was performed using a HP5890 II instrument with an MSSV injector and an FID. The column is a HP-1 (length 50 m, i.d. 0.32 mm, film thickness 0.52 μm) and the injector unit is from Margot Köhnen-Willsch Chromatographie & Software. An open sample tube containing 20 mg of pulverized whole rock was placed in the system injector at a preheated temperature of 300 °C and volatile compounds evaporated before the pyrolysis oven was closed. The oven temperature was increased to 600 °C at a rate of 25 °C/min. The pyrolysis products were collected in a liquid nitrogen-cooled trap for 10 min before being released into the GC column, whereupon there were released at an initial temperature of 40 °C (held 13 min), heated to 300 °C at 5 °C/min (held 25 min), and finally increased to 320 °C at 5 °C/min (held 10min). The pyrolysates were monitored on-line using a HP-1 capillary column (length 50m, i.d. 0.32 mm, film thickness 0.52 μm) on the GC that was equipped with a flame ionization detector (FID). Boiling ranges (C1, C2–C5, C6–C14, C15+) and individual compounds (n-alkenes, n-alkanes, alkylaromatic, and alkylthiophenes) were quantified using n-butane as an external standard. Response factors for all resolved compounds were assumed to be the same. In the case of methane, a response factor of 1.1 was assumed according to di Primio et al. (1998).

To constrain bulk kinetic parameters of primary kerogen to petroleum transformation, the 15 samples were subjected to non-isothermal open-system pyrolysis at five different heating rates (1 °C/min, 2 °C/min, 5 °C/min, 15 °C/min, 25 °C/min) using a Rock-Eval 6 instrument. Kinetics05 software from Lawrence Livermore National Laboratory (Burnham et al., 1987) was used to calculate a discrete activation energy distribution (E_A) and the frequency factor (A).

Non-isothermal, closed system pyrolysis-gas chromatography using micro-scaled sealed vessels (MSSV Closed-System Pyrolysis) was used for compositional kinetic modeling following the approach described by Horsfield et al. (1989) and Dieckmann and Keym (2006). Milligram amounts of five selected samples were sealed in glass capillary tubes (five tubes per sample) and heated at a single heating rate (0.7 °C/min) to final temperatures corresponding to preselected transformation ratios (10%, 30%, 50%, 70% and 90%). The temperatures corresponding to the selected transformation ratios were determined by simulated heating of the bulk kinetics parameters, as estimated from the Rock-Eval pyrolysis data, at the specified heating rate. The sample tubes were placed in the injector system and then broken when pressure had stabilized after 4 min. The composition of the generated hydrocarbon products was analyzed by thermovaporisation-gas chromatography (Tvap-GC) as described above. Compositional models with two (oil and gas), four (C_1, C_2–C_5, C_6–C_{14} and C_{15+}), and fourteen (C_1, C_2, C_3, i-C_4, n-C_4, i-C_5, n-C_5, pseudo-C_6, C_7–C_{15}, C_{16}–C_{25}, C_{26}–C_{35}, C_{36}–C_{45}, C_{46}–C_{55}, C_{56}–C_{80}) components were developed.

For prediction of petroleum physical properties such as saturation pressure (P_{sat}), gas to oil ratio (GOR), and formation volume factor (B_o), the Phase Kinetics approach by di Primio and Horsfield (2006) was followed. The estimation of petroleum phase was carried out using the fluid description consisting of 14 components, seven in the gas range (C_1, C_2, C_3, i-C_4, n-C_4, i-C_5, n-C_5) and seven in the liquid range (pseudo-C_6, C_7–C_{15}, C_{16}–C_{25}, C_{26}–C_{35}, C_{36}–C_{45}, C_{46}–C_{55}, C_{56}–C_{80}; di Primio and Horsfield, 2006).

The composition of pyrolysis gases differs substantially from natural gas (Mango, 1996, 2000, 2001). The most important difference is the comparably low content of methane in gases derived from pyrolysis experiment (di Primio and Horsfield, 2006). Methane is known to have the highest impact on the phase behavior (di Primio et al., 1998; di Primio and Skeie, 2004) and, therefore, its relative abundance needs to be corrected following the approach by di Primio and Horsfield (2006). The correcting procedure consisted in iterative adjustment of the methane to wet gas ratio, assuming decreasing gas wetness ratio for increasing transformation ratio, and shifting of the trends of P_{sat} against GOR and P_{sat} against B_o closer to the linear trends typically observed in natural petroleum systems (di Primio and Horsfield, 2006). The properties of the C_{7+} lumped fractions were then calculated from the corresponding properties for C_7 to C_{80} single carbon number groups by mass weighted averaging as described by Pedersen et al. (1985). The tuned component descriptions from MSSV closed-system pyrolysis were combined with the bulk kinetic model from open-system pyrolysis. The 14 components were allocated to the non-zero reaction weights from the bulk kinetic model, so that simulation of the resultant 14-component kinetic model best-fits the MSSV data. A coordinate-wise stochastic search algorithm (Zabinsky et al., 1993; Zabinsky, 1998) was used to compute a least-squares best-fit of the compositional kinetic model to the tuned compositional descriptions.

It is instructive to highlight that the accurate prediction of natural fluid properties is limited by the fundamental difference between the bulk composition of naturally generated petroleum and that of kerogen pyrolysates regardless of kerogen type or pyrolysis techniques (Karlsen and Larter, 1991; Larter and Horsfield, 1993; Horsfield, 1997). Natural oils are hydrocarbon-rich systems, while pyrolysates consist of comparatively higher proportions of aromatic and polar compounds (Urov, 1980; Castelli et al., 1990; Karlsen and Larter, 1991).

4. Results

4.1. Rock-Eval, TOC, and maceral assemblages

The TOC contents of the fifteen source rock samples selected for artificial maturation experiments range from 2.2 to 23 wt% with HI values in the range of 115–378 mg HC/g TOC (Table 1). High HI values are mostly associated with elevated TOC contents, while comparatively lower HI values correspond to low TOC contents (Fig. 3A). Sample H from well 7220/5-2 has a HI value of 378 mg HC/g TOC paired with a relatively low TOC content of 2.4% and, therefore, deviates from the main trend. When plotted on the pseudo-Van Krevelen diagram, the HI data indicates the presence of various proportions of mixed kerogen types II and III (Fig. 3B).

The investigated samples have not reached thermal stress levels required for petroleum generation and expulsion as indicated by their T_{max} Rock-Eval temperatures that are mostly equal or lower than 426 °C (Table 1). A T_{max} value of 432 °C was reported for sample E; however, based on its high relative abundances of thermally stable vitrinites (Table 1), it is interpreted to retain most of the original generative potential. Thus, the variations in TOC, HI, and maceral composition are expected to be primarily related to organic facies. This study did not find any detectable changes in the pyrolysis-gas chromatography data resulting from maturity variations in the sample set (i.e. T_{max} = 403–432 °C) that may affect the interpretations.

The maceral composition of the investigated samples comprises a wide range of assemblages ranging from terrestrial dominated (i.e. vitrinite and terrestrial-derived liptinite) to marine dominated (i.e. marine-derived liptinite) (Table 1). Fragments of detrovitrinite and primary vitrinite constitute the bulk of the vitrinite group, whereas sporinite, and only occasionally cutinite and resinite, predominates in the terrestrial liptinite sub-group. The marine liptinite sub-group consists mainly of

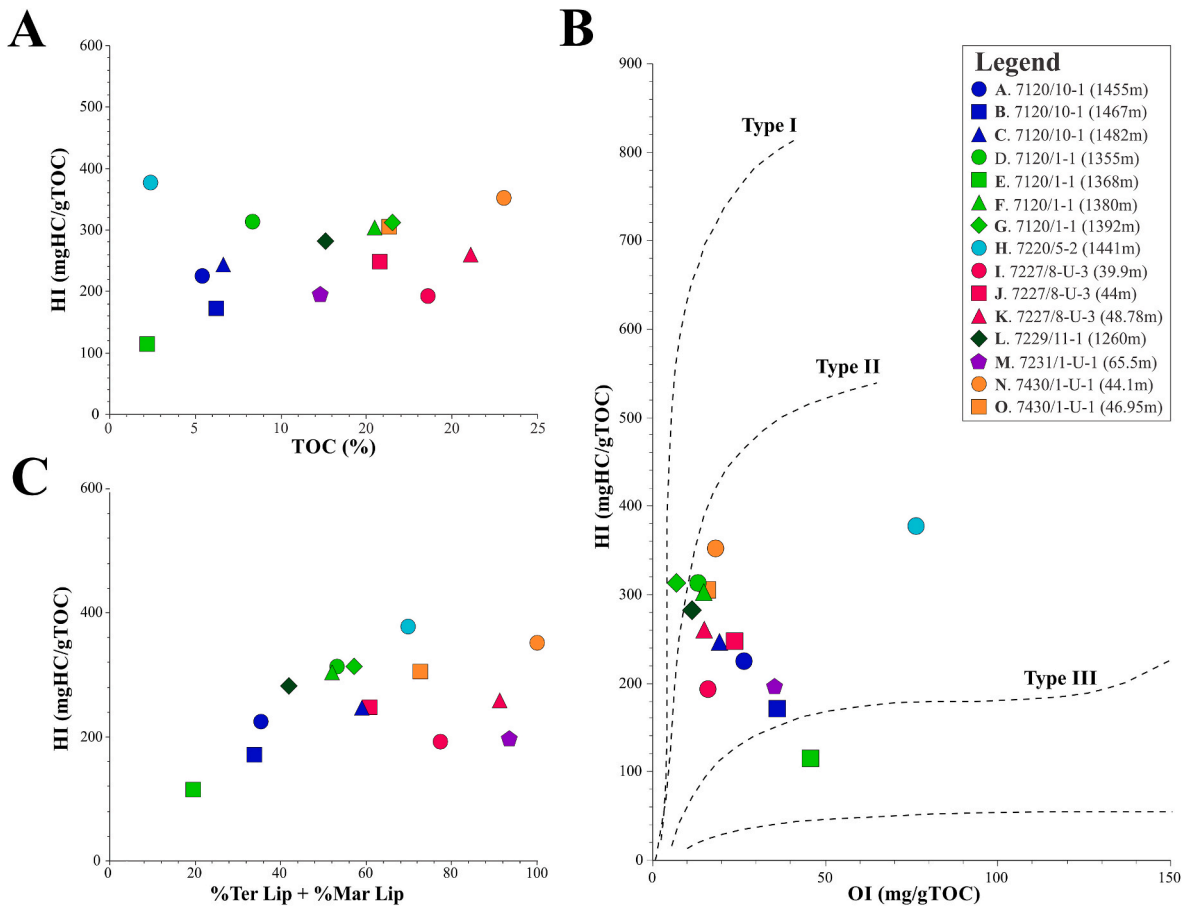

Fig. 3. Total organic carbon (**A**), oxygen index (**B**), and liptinites (**C**) versus hydrogen index cross-plots of studied samples. Maturation pathways for the three main kerogen types in plot B are shown after Cornford (1998).

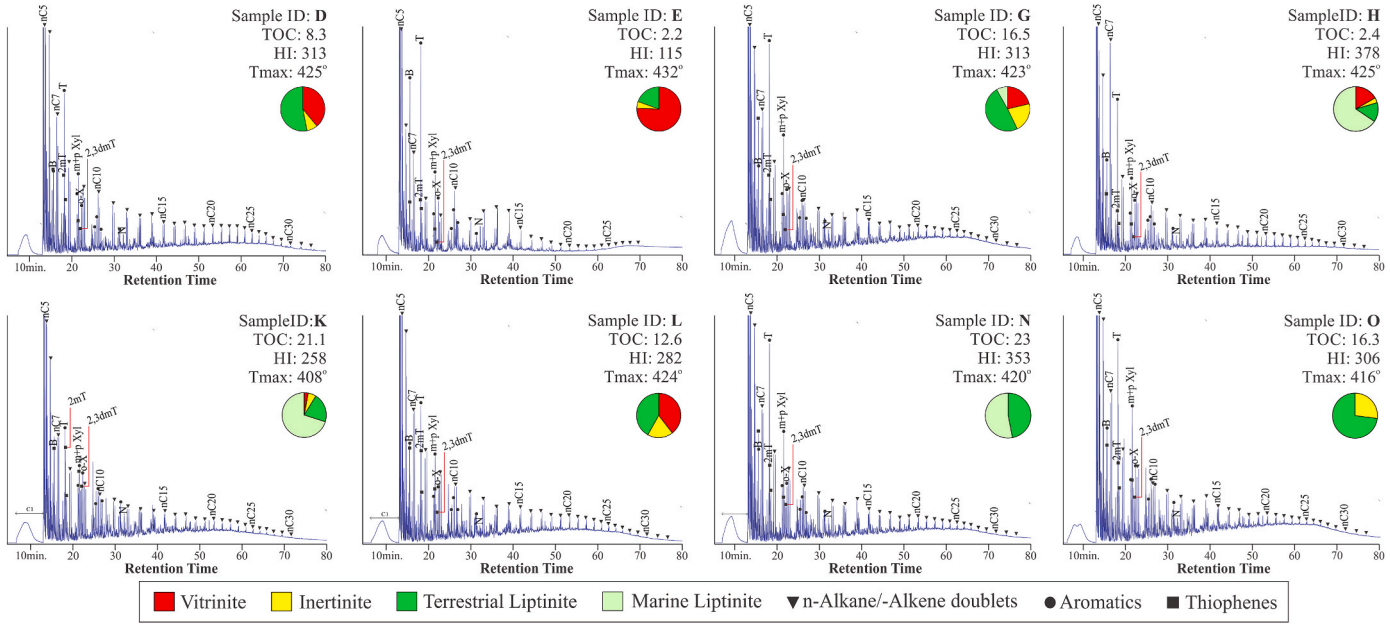

Fig. 4. Representative pyrolysis–gas chromatograms of eight selected source rocks samples. B = benzene, T = toluene, 2 mT = 2-methyl-thiophene, m + p xylene = meta + para-xylene, 2,3dmT = 2,3 dimethyl-thiophene, o-X = ortho-xylene, N = naphthalene. TOC = total organic carbon - wt%; HI = hydrogen index – mgHC/gTOC; Tmax = Tmax Rock-Eval - °C.

alginite particles (i.e. lamalginite, tasmanites, dinoflagellates). Only sample H contains elevated amounts of amorphinite, a marine kerogen maceral known to possess a high oil-proneness. A positive correlation between HI and liptinites is shown in Fig. 3C. The low to only modestly high hydrogen richness in the studied samples is coincident with the elevated inputs of autochthonous terrestrial inputs (see Cedeño et al., 2021).

4.2. Predicted petroleum type from Py-GC

Open system pyrolysis gas chromatography (Py-GC) was conducted on fifteen selected samples with distinctive maceral assemblages (Table 1) to characterize the macromolecular composition of kerogen pyrolysates and predict the generated petroleum types. Boiling ranges for C_1, C_2–C_5, C_6–C_{14} and C_{15+} and individual compounds were quantified up to n-C_{32} for most of the sample set (Fig. 4). Straight-chain aliphatic hydrocarbons, i.e. n-alkane/n-alkene doublets, dominate the pyrolysate. There is a systematic decrease in abundance of n-alkane/n-alkene doublets with increasing carbon number in the Py-GC traces. The precursors of aliphatic hydrocarbons in the source rock kerogens could be lipids inherited from aliphatic biopolymers (Tegelaar et al., 1989) or lipids incorporated through either condensation reactions (Tissot and Welte, 1984) or quenching of labile functionalized lipids with inorganic sulfur acting as a reactant during early diagenesis (Sinninghe Damste et al., 1989).

Besides aliphatic hydrocarbons, the most prominent individual compounds in the pyrolysate are, in descending order, mono-aromatic hydrocarbons (i.e. benzene, alkylbenzenes, trimethylbenzenes), sulfur-containing compounds (i.e. mostly alkylated thiophenes), and di-aromatic hydrocarbons (i.e. naphthalenes and methylnaphthalenes) (Fig. 4). Relatively high abundance of mono-aromatic hydrocarbons is often linked with terrestrial organic inputs (Tissot and Welte, 1984; Horsfield et al., 1992). In this study, such an assertion is supported by the relative abundance of toluene being greater than the C_7 n-alkyls in the more terrestrially-influenced samples (Fig. 4E), but are of similar or lower abundance in the marine liptinitic samples (Fig. 4H). Other mono-aromatic compounds such as benzene and meta + para-xylene sometimes occur in greater abundance than n-alkyls of the same carbon numbers. The most and least prominent thiophene compounds are 2-methyl-thiophene and 2,3-dimethylthiophene, respectively, but these are overall less abundant than the corresponding n-alkyls.

The amount of thiophenes generated during thermal degradation of kerogen under open-system pyrolysis can be used to assess the organic sulfur content of the organic matter (Eglinton et al., 1990). The ternary diagram in Fig. 5A uses a sulfur-bearing (i.e. 2,3-dimethylthiophene), an aromatic (i.e. ortho-xylene) and an aliphatic compound (i.e. n-alkene n-C9:1) for discriminating between freshwater lacustrine (Type I), terrestrial (Type III), clay-rich marine (Type II) and sulfur-containing carbonated environments (Type IIS). Twelve of the pyrolyzed samples yield varyingly low amounts of sulfur-bearing compounds, whereby they plot in the sulfur-poor kerogen type II and III fields. Kerogen pyrolysates falling in the kerogen type II field typically contain 50% by volume liptinitic macerals, either marine or terrestrial, and HI values generally higher than 250 mg HC/g TOC (Table 1). The pyrolysate products from sample E plot well into the kerogen type III field. This is consistent with the high concentrations of humic kerogen of a vitrinitic nature (i.e. 76%) and the very low HI value of 115 mg HC/g TOC (Table 1).

The kerogen pyrolysates of samples J, K, and L possess higher sulfur contents as compared to the other samples and plot in, or close to, the type IIS field (Fig. 5A). Pyrolysates with this relatively high thiophenic sulfur abundance are typically associated with clay-poor source rocks containing sulfur-rich kerogens (i.e. type IIS; Tissot et al., 1987; Eglinton et al., 1990; Braun et al., 1991; Tegelaar and Noble, 1994; Schaeffer et al., 1995; Orr, 1986; di Primio and Horsfield, 1996; Hartwig et al., 2012). The clastic mineralogy reported for these samples (Table 1) fails to support the composition derived from their pyrolysates. It is possible that the elevated concentration of 2,3-dimethylthiophene resulted from the early elimination of organically-bound sulfur occurring naturally in some terrestrial-derived materials (Eglinton et al., 1990, 1992). Alternatively, such a high concentration of thiophenic sulfur could originate from diagenetic incorporation of inorganic sulfur into unsaturated and functionalized lipids in the kerogen (i.e. sulfurization; Kaplan et al., 1963; Sinninghe Damste et al., 1989; Tegelaar et al., 1989; Eglinton et al., 1992).

The n-alkyl chain length distribution derived from source rocks during open system pyrolysis can be used to predict the likely petroleum types they generate throughout the entire natural maturation sequence (Horsfield et al., 1989; Horsfield, 1997). The ternary plot in Fig. 5B employs the total light gas fraction (i.e. Σ nC_1-C_5) and the intermediate (i.e. Σ n-C_6-C_{14}) and long-chained (i.e. Σ n-C_{15+}) n-alkyls to discriminate paraffinic (low and high wax varieties), paraffinic-naphthenic-aromatic (P–N-A) (low and high wax varieties), and the gas & condensate petroleum generating potentials. Based on the n-alkyl chain length distribution, most of the investigated samples are predicted to generate gross pyrolysates that fall within the Low Wax P–N-A oil generating facies.

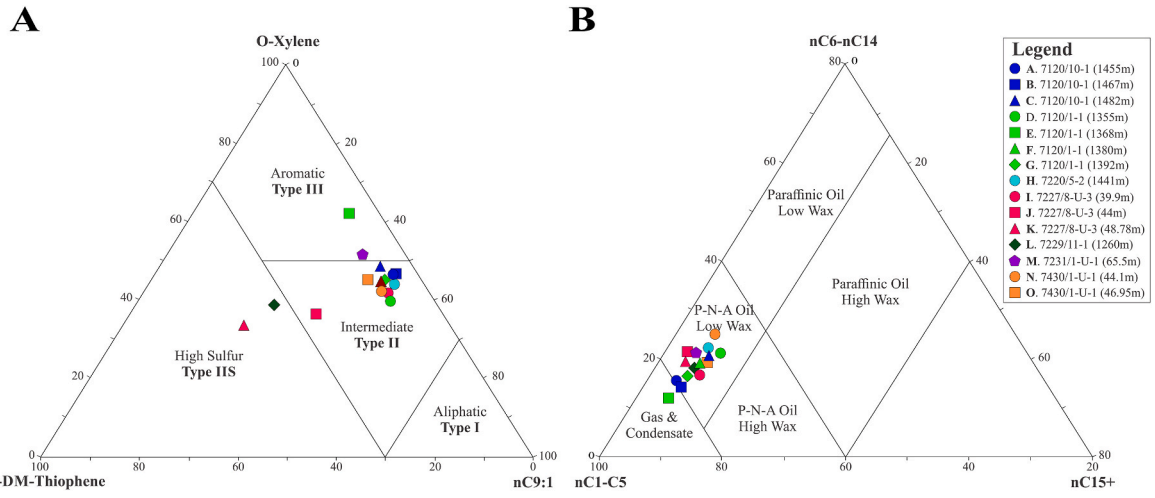

Fig. 5. A. Ternary diagram of n-C9 alkene (n-C9:1), ortho-xylene (O-Xylene), and 2,3 dimethyl-thiophene (2,3-DM-Thiophene) used for kerogen classification according to Eglinton et al. (1990). **B.** Ternary diagram of total C1–C5, C6–C14, and Σ n-C15+ n-alkanes + n-alkenes used for petroleum type prediction according to Horsfield et al. (1989).

Samples plotting well into the Low Wax P–N-A oil facies are compositionally rich in liptinitic particles. Only sample E plots in the gas and condensate field, whereas samples A and B plot on, or near, the boundary between the gas & condensate and Low Wax P–N-A fields. The higher proportions of short chained compounds in these samples are consistent with their high vitrinite contents and low HI values of 115, 171, and 225 mg HC/g TOC, respectively.

4.3. Kinetic models of bulk petroleum generation

Bulk kinetics analysis using non-isothermal open-system pyrolysis was performed to model the kinetic parameters, i.e. activation energy distribution and frequency factor, of bulk petroleum generation. The majority of the computed kinetic models show activation energies in the range of 45–70 kcal/mol (Table 2), with a gaussian-like shape (Fig. 6) commonly associated with marine-influenced kerogens (Braun et al., 1991; Tegelaar and Noble, 1994). This broad E_A reflects large variability in the composition of the organic constituents, intrinsically comprising a wide spectrum of chemical bond types and strengths. Associated frequency factors range between 2.80E+13/s and 1.96E+16/s (Table 2). The sample set was divided into three sub-sets according to the volumetrically predominant maceral (i.e. marine liptinites, terrestrial liptinites, vitrinites) and an average E_A distribution was computed for each sub-set. The average E_A distributions are displayed in Fig. 7 for the purpose of comparing the variability in activation energies linked to maceral compositions.

It is generally accepted that marine-rich kerogens often require lower activation energies than do terrestrial-rich kerogens (i.e. type II kerogen versus type III kerogens) to generate petroleum. This organic matter dependance in the present study is reflected in the fact that the lowest activation energy distributions occur in samples containing high relative abundances of marine liptinites, and increase gradually with increasing contents of terrestrial macerals (Fig. 6; Table 2). Samples K, H, and N, in which liptinites of marine origin account for 70%, 66% and 53%, have peak activation energies at 52 kcal/mol, 53–54 kcal/mol and 54 kcal/mol, respectively.

The more terrestrially influenced samples G, D, and E have activation energy maxima at 58 kcal/mol, 59 kcal/mol, and 60–61 kcal/mol, respectively (Fig. 6). The organic fraction (i.e. kerogen) in samples E and G is predominantly composed of vitrinite and terrestrial liptinite, respectively, while the kerogen in sample D has an intermediate composition. In comparing their maceral composition and their activation energy distributions, it is apparent that the vitrinite-rich sample requires slightly higher activation energies than the liptinite (terrestrial)-rich sample. This is further substantiated by Fig. 7 in which activation energy distributions of other vitrinitic kerogens in the sample set show dominant peaks between 59 and 61 kcal/mol compared to maxima between 56 and 59 kcal/mol recorded for the terrestrial liptinitic kerogens. It is interesting to note that the activation energy distribution of the more terrestrially influenced samples is overall broader than the more marine influenced samples. These observations reflect the more heterogeneous molecular composition of terrestrial organic matter compared to the marine organic matter (Tissot et al., 1987; Reynolds and Burnham, 1995; Schenk et al., 1997; Petersen and Rosenberg, 2000).

The low range of activation energies in sample L is an oddball among the data set. This sample is exclusively composed of terrestrial macerals yet exhibits a peak activation energy at 52 kcal/mol, 53 kcal/mol, and 54 kcal/mol (Fig. 6). This attribute could be the result of inorganic sulfur incorporation in reducing kerogen stability, as discussed in section 4.2.

4.4. Petroleum formation and timing predictions

The derived kinetic parameters provide the basis to estimate the temperatures of bulk petroleum generation and corresponding transformation ratio (TR; Fig. 8). A constant heating rate of 3.3 °C/Ma was assumed to extrapolate to geological heating conditions. The variability described in activation energy distributions and frequency factors is manifest in the temperatures at which the onset and peak petroleum generation occur. In Fig. 8, the onset of significant petroleum generation (10% TR) from least to most thermally stable kerogen varies from 123 °C to 144 °C. This temperature difference of up to 21 °C equates to a difference of up to 700m of burial if a geothermal gradient of 30 °C is assumed. These relatively high and different orders of thermal stability are consistent with the previously discussed mixtures of terrestrial and marine organic materials. A similar temperature range of 25 °C is observed at the peak of petroleum generation (i.e. 70 % TR), reflecting the involvement of relatively similar cracking reactions and conversion rates with increasing thermal stress regardless of the samples' different activation energy distributions and frequency factors.

The onset and peak petroleum generation from the more marine-influenced source rocks K, H, and N is predicted to occur at the lowest temperatures of 123 °C and 150 °C, respectively (Fig. 8). The early, low-temperature generation in these samples seems to be related with the

Table 2
Bulk kinetic parameters (i.e. activation energies and frequency factors) of the fifteen studied samples.

ID	A	B	C	D	E	F	G	H	I	J	K	L	M	N	O
Well	7120/10-1	7120/10-1	7120/10-1	7125/1-1	7125/1-1	7125/1-1	7125/1-1	7220/5-2	7227/8-U-3	7227/8-U-3	7227/8-U-3	7229/11-1	7231/1-U-1	7430/10-U-1	7430/10-U-1
Depth	1455	1467	1482	1355	1368	1380	1392	1441	39.9	44	48.75	1260	65.5	44.1	47.08
A s-1	6.4058E+15	1.71174E+16	5.5906E+14	7.5211E+15	1.27656E+16	1.494E+15	5.2015E+15	1.3701E+14	1.132E+16	2.0104E+15	2.8073E+13	1.3343E+14	1.9602E+16	3.2549E+14	1.7673E+15
Ea (kcal/mol)															
40	0.0	0.0			0.1					0.0					
41	0.0	0.0			0.0					0.0					
42	0.0	0.0			0.0					0.0				0.0	
43	0.0	0.0			0.0					0.0	0.0			0.0	
44	0.0	0.0			0.0			0.0		0.1	0.0			0.0	
45	0.0	0.0	0.0		0.0			0.4		0.0	0.1			0.0	
46	0.0	0.1	0.0		0.0			0.3		0.0	0.0			0.0	
47	0.0	0.0	0.0		0.1			0.7		0.2	0.9			0.2	
48	0.0	0.0	0.2	0.0	0.0			0.7		0.0	0.9			0.2	
49	0.0	0.0	0.1	0.0	0.0	0.0		2.2		0.4	1.5			0.0	
50	0.1	0.1	0.0	0.1	0.1	0.1	0.0	0.5		0.3	8.8			0.6	0.0
51	0.0	0.0	0.5	0.0	0.3	0.1	0.0	4.8		1.2	19.2	0.0	0.0	2.8	0.7
52	0.3	0.3	0.3	0.1	0.0	0.0	0.2	4.9		1.7	29.5	24.0	0.2	11.5	0.6
53	0.3	0.1	6.0	0.6	0.6	0.5	0.0	30.9	0.0	4.9	11.8	20.9	0.0	14.3	5.0
54	0.0	1.0	14.7	0.0	0.4	6.0	0.0	31.2	1.2	7.9	12.3	25.1	1.6	26.2	11.9
55	0.9	0.2	25.2	0.4	1.1	16.4	1.3	11.4	2.9	15.1	6.9	10.6	1.9	19.5	9.1
56	2.6	2.9	20.3	0.4	1.9	22.5	8.4	5.4	10.8	18.6	1.2	10.9	5.9	10.2	33.8
57	10.4	6.1	14.4	8.1	4.2	19.5	17.8	4.3	17.3	21.3	2.5	0.1	10.2	7.2	18.1
58	19.6	12.8	7.6	17.4	6.9	13.5	22.3	1.7	19.1	15.6	1.4	5.9	14.9	1.2	11.0
59	22.6	18.9	2.3	23.4	15.0	8.6	17.9	0.1	18.1	6.2	0.2	0.7	18.9	2.6	4.6
60	17.1	20.2	6.3	17.6	18.8	5.0	11.2	0.0	13.0	4.2	0.7	0.7	23.3	0.5	1.8
61	11.8	15.0	0.2	14.0	17.9	1.6	8.3	0.0	7.4	1.6	0.0	0.7	13.5	1.4	1.3
62	3.7	10.5	1.4	7.2	13.5	4.0	4.2	0.0	4.4	0.1	0.0	0.1	5.8	0.0	0.9
63	4.4	4.8	0.1	1.7	8.3	0.2	1.7	0.6	1.3	0.4	0.0	0.2	1.4	0.8	0.3
64	4.4	2.0	0.6	5.8	4.5	1.1	4.0		2.4	0.0	2.1	0.0	1.5	0.1	0.4
65	0.0	3.3	0.0	0.0	1.5	0.3	0.4		0.5	0.0		0.0	0.1	0.1	0.0
66	1.0	0.9		1.3	3.3	0.0	0.8		0.5	0.0		0.2	0.4	0.5	0.3
67	0.3	0.2		0.9	0.6	0.1	0.7		0.5	0.0			0.0	0.0	0.0
68	0.0	0.0		0.0	0.0	0.1	0.0		0.0	0.0			0.1	0.0	0.0
69	0.1	0.5		0.0	0.8	0.4	0.0		0.0	0.0			0.2	0.0	0.0
70	0.5			0.3			0.4		0.3				0.0		0.3
71	0.0			0.0			0.0		0.1				0.0		
72	0.0			0.9			0.4		0.2				0.0		

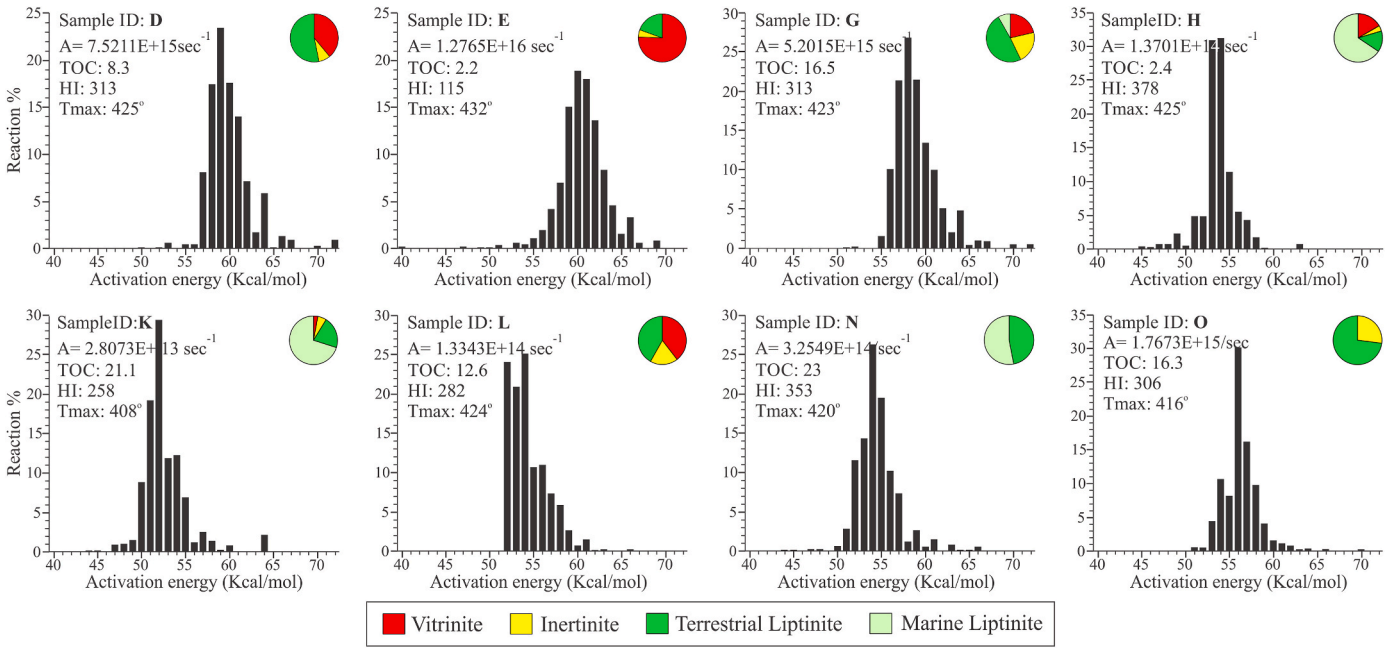

Fig. 6. Activation energy distribution of eight selected source rock samples. Pie diagrams represent the maceral composition of the corresponding sample. TOC = total organic carbon - wt%; HI = hydrogen index – mgHC/gTOC; Tmax = Tmax Rock-Eval - °C.

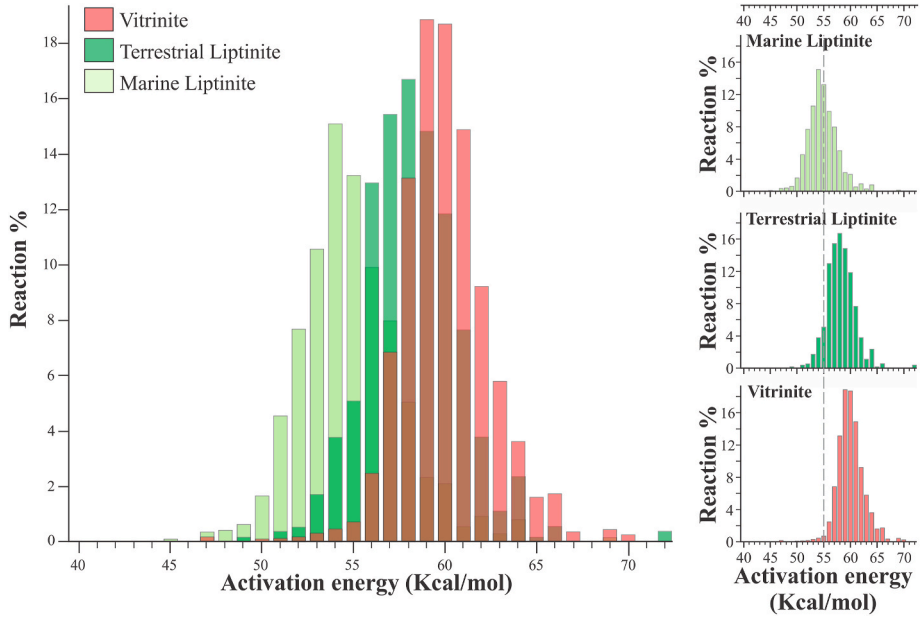

Fig. 7. Average activation energy distributions computed according to the volumetrically predominant maceral (i.e. marine liptinites, terrestrial liptinites, vitrinites) in each sample. Vitrinite subset = A, B, E; terrestrial liptinite subset = D, G, I, J, M, N; marine liptinite subset = C, F, H, K, N.

abundance of thermally labile marine particles. Sample K, interpreted to be enriched in thiophenic sulfur according to Fig. 5A, reaches onset and peak generation at temperatures within the same range as the other two sulfur-poor source rocks. This indicates that in this particular case sulfur richness has a minor impact on the timing of petroleum formation. Kinetic information from an average Type II North Sea (Tegelaar and Noble, 1994) and Type IIS source rock from the Campeche Basin (Santamaria Orozco, 2000) are plotted in Fig. 8 for comparison purposes.

Petroleum generation from source rock samples dominated by terrestrial macerals takes place at higher temperature ranges relative to marine-influenced sources. The onset of generation is predicted to occur at temperatures ranging from 139 °C for sample G to 144 °C for sample E (Fig. 8). The gas and condensate-prone sample E displays the highest stability at 70 and 90% conversion (i.e. generating petroleum up to 190 °C) as well as the broadest temperature range of generation. This demonstrates the slower conversion rates typically associated with vitrinitic type III kerogens.

In the case of the sulfur-rich L and J source rock samples, onset and peak generation occur at least 10 °C earlier than in other samples containing comparable maceral assemblages (Fig. 8). This generation at relatively low levels of maturity could be attributed to the break-down of weak carbon-sulfur bonds under less intense thermal stress (i.e. Orr, 1986; Tissot et al., 1987; di Primio and Horsfield, 1996; Van Dongen et al., 2003). The apparent lack of front-end activation energies in

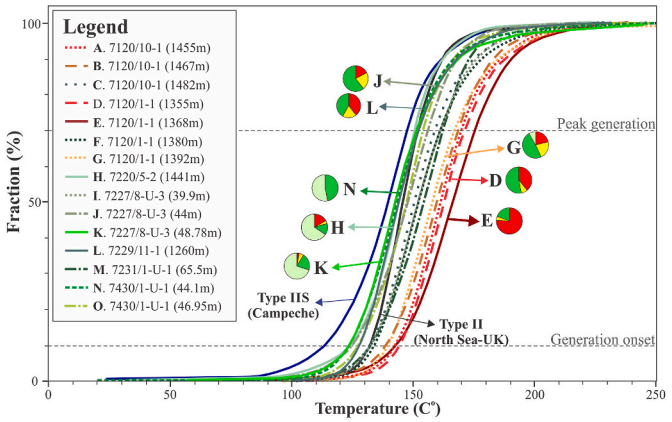

Fig. 8. Transformation rate curves calculated from bulk kinetic models of the sample set. A geological heating rate of 3.3 K/Ma is assumed. Relevant samples discussed in the text and corresponding kerogen compositions are displayed. The main petroleum generation events are shown. Transformation rate curves for a typical North Sea Type II kerogen (Tegelaar and Noble, 1994) and Type IIS kerogen from the Campeche Basin (Santamaria Orozco, 2000) are plotted for comparison purposes.

sample L (Fig. 6) implies that petroleum generation may have commenced at subsurface temperatures equivalent to Tmax values ≤ 424 °C (Table 1).

4.5. The PhaseKinetics approach: compositional kinetic models and fluid physical properties

The PhaseKinetics approach as defined by di Primio and Horsfield (2006) provides the basis to predict the compositional evolution and the physical properties (i.e. GOR, Bo, and Psat) of the generated fluids with increasing maturity. The five samples for MSSV-Py-GC-FID experiments were selected to represent most of the variability in maceral assemblages and kinetic parameters across the broader sample set. Three compositional models were constrained based on two components (C_1–C_5 and C_{6+}), four components (C_1, C_2–C_5, C_6–C_{14}, and C_{15+}), and 14 components (C_1, C_2, C_3, i-C_4, n-C_4, i-C_5, n-C_5, n-C_6, C_7–C_{15}, C_{16}–C_{25}, C_{26}–C_{35}, C_{36}–C_{45}, C_{46}–C_{55}, and C_{56}–C_{80}) (Table 3). The compositional kinetic models with 14 components are presented in Fig. 9.

Table 3
Compositional kinetic models with 2, 4, and 14 components calculated for five selected samples. Potentials are shown in weight percentage (wt-%).

ID	D	H	L	N	O
Well	7125/1-1	7220/5-2	7229/11-1	7430/10-1-3	7430/10-1-3
Depth	1355 m	1441 m	1260 m	44.1 m	46.95 m
Oil	65.0	63.7	67.7	74.7	74.1
Gas	35.0	36.3	32.3	25.3	25.9
C1	13.1	14.1	12.1	9.9	9.6
C2-C5	21.9	22.2	20.2	15.4	16.3
C6-C15	44.9	45.4	42.9	43.4	47.7
C15+	20.0	18.3	24.8	31.3	26.4
C1	13.1	14.1	12.1	9.9	9.6
C2	5.8	6.4	5.4	4.4	4.0
C3	6.1	5.7	5.8	4.6	4.5
iC4	1.2	1.6	1.1	1.0	0.8
nC4	3.7	4.1	3.7	3.2	2.9
iC5	2.5	2.1	1.9	1.5	2.0
nC5	2.8	2.3	2.3	0.8	2.0
C6	4.2	3.9	3.7	3.8	4.0
C7-15	40.8	41.5	39.2	39.6	43.7
C16-25	16.5	15.7	20.3	23.0	20.3
C26-35	3.0	2.3	3.7	5.7	4.7
C36-45	0.5	0.3	0.7	1.8	1.1
C46-55	0.1	0.0	0.1	0.6	0.2
C56-80	0.0	0.0	0.0	0.3	0.1

Hydrocarbons with six or more carbons ($\geq C_{6+}$) comprise 63.7 to 74.7 wt% of the total pyrolysates (Table 3). The remaining pyrolysate yield is composed of gaseous hydrocarbons (C_1–C_5). These compositional attributes show that the studied samples are capable of generating fluid and, in less proportions, gaseous hydrocarbons. Source rock samples N and O from well 7430/10-U-1 have the highest liquid generative potential with 74.7 and 74.1 wt%, respectively, but possess different kerogen maceral compositions. The shallower sample contains about equal amounts of marine and terrestrial liptinites (53% and 47%, respectively), while the deeper sample contains mostly terrestrial liptinite (73%; Table 1). Samples D, L, and H generate comparatively lower proportions of liquid hydrocarbons (65, 67.7 and 63.7 wt%, respectively). Sample H features an elevated abundance of marine-derived liptinites (66%) and similar amounts of vitrinite and terrestrial liptinite, whilst samples D and L possess exclusively terrestrial macerals in comparable proportions.

The n-C_7–C_{35} fraction constitutes most of the liquid portion of these Low Wax P–N-A oils (Table 3). Nevertheless, a closer look at the 14-component compositional kinetic models reveals distinct generative potentials within the liquid fraction. The lighter C_7–C_{15} liquids in the least oil-prone samples D, H, and L account for 62.1, 67.6, and 69.7 wt% of the n-C_7–C_{35} compositional fraction compared to lower values of 58 and 63.6 wt% in the most oil-prone samples (i.e. N, O). A waxier character of the most oil-prone samples is also manifest in a relative enrichment in the heavier C_{26}–C_{35} and C_{36}–C_{80} potentials (Table 3).

Predicted GORs, P_{sat}, and B_o of petroleum fluids increase as a function of increasing TR in all cases (Fig. 10; Table 4). The H source rock sample exhibits the highest GORs at all transformation ratios (Fig. 10A). It generates black oils (GOR <350 standard m3/m3) at TRs of 10 and 70% and light oils (350 < GOR <600 m3/m3) at TR of 90%. Additionally, this sample displays the highest gas generative potential (36.3 wt%; Table 3), which is consistent with the high GORs, P_{sat}, and B_o. The remaining samples display consistently lower GOR values with only black oils generated, except for some potential for light oils at late TR in sample D. This increase in GOR at higher conversion rates can be ascribed to either late generation of primary gas resulting from the breakdown of thermally stable vitrinites or to the initiation of secondary cracking of trapped gas with increasing thermal stress (Dieckmann et al., 1998). The most oil-prone samples from well 7430/10-U-1 (N and O) generate petroleum fluids with the lowest GORs, P_{sat}, and B_o values in this data set (Fig. 10; Table 4). This condition is consistent with their comparatively low gas generation potentials (25.3 and 25.9%, respectively; Table 3) and their waxier composition.

5. Discussion: organic facies variations and their impact on petroleum generation in the Barents Sea

5.1. Vertical organic facies variations

Pyrolysis data from well 7125/1-1 in the Nysleppen Fault Complex illustrates variations in thermal stability and geochemical composition inherited from differences in organic facies (Fig. 11B). Peak activation energies occur between 55 and 57 kcal/mol and 59–62 kcal/mol in the marine liptinite-rich (1380m, i.e. sample F) and the vitrinite-rich sample (1368m, i.e. sample E), respectively. As a consequence of the strong vitrinitic input, the latter sample has the potential to generate gas & condensate, whereas the remaining liptinitic kerogens (i.e. D, F, and G) generate intermediate, P–N-A low wax oils (Fig. 5). The bulk of the organic fraction throughout well 7120/10–1 consists of land-plant derived materials with comparable generation potentials (e.g. similar HI values) and peak activation energies at 59–60 kcal/mol (Fig. 11A). A moderate increase in the content of marine macerals at 1482m (i.e.

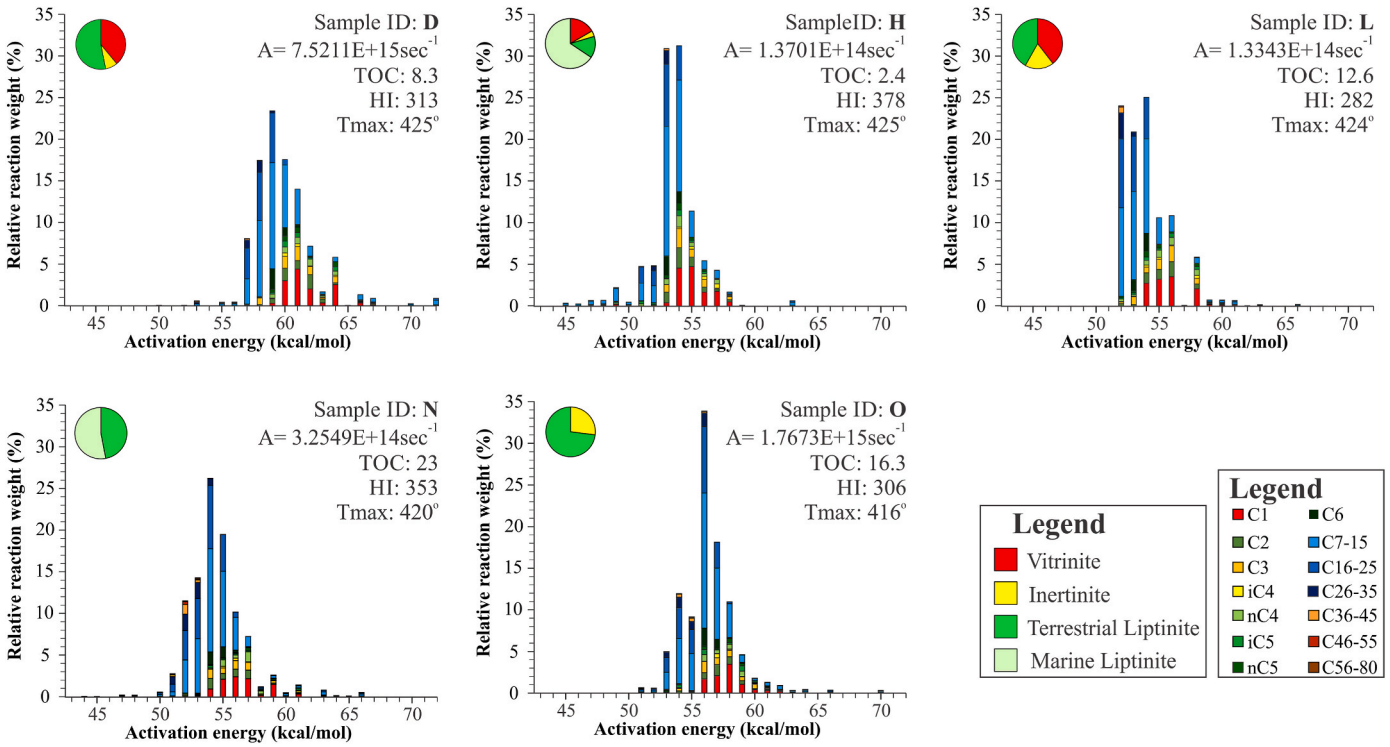

Fig. 9. Compositional kinetic models with fourteen components for five source rock samples. Pie diagrams represent the maceral composition of the corresponding sample. TOC = total organic carbon - wt%; HI = hydrogen index – mgHC/gTOC; Tmax = Tmax Rock-Eval - °C.

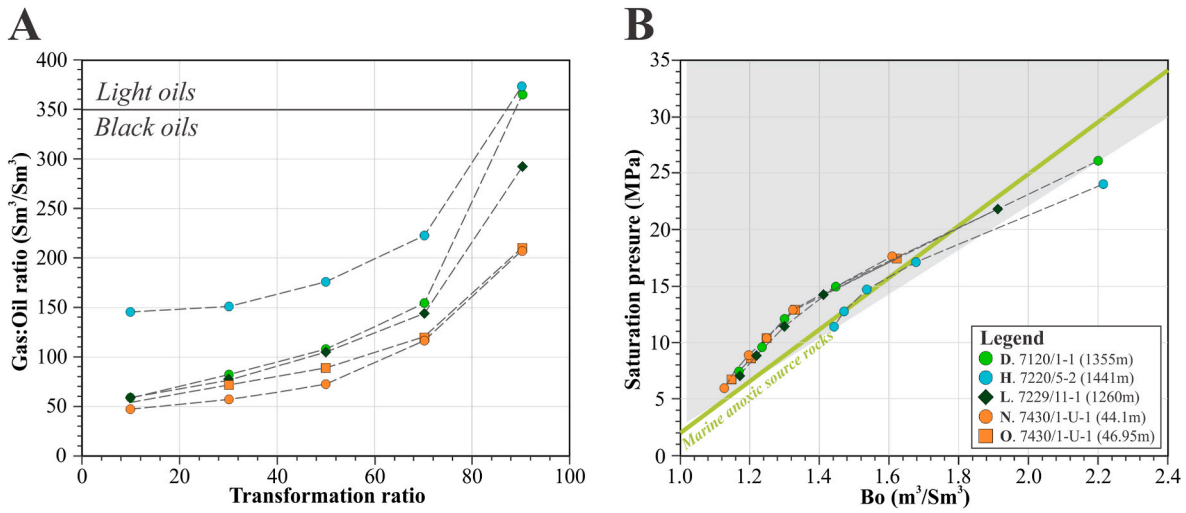

Fig. 10. Evolution of physical properties (i.e. gas to oil ration = GOR, volume factor = Bo, and saturation pressure = Psat) of generated fluids with increasing maturity calculated from micro-scaled sealed vessels (MSSV Closed-System Pyrolysis) experiments using the PhaseKinetics approach as defined by di Primio and Horsfield (2006). **A.** Cross-plot of transformation ratio versus GOR. **B.** Cross-plot of Bo versus Psat. The light grey area corresponds to naturally occurring petroleum fluids according to di Primio and Horsfield (2006).

sample C) causes the activation energy distribution to peak at 55–56 kcal/mol, and hence, 70% conversion takes place around 10 °C earlier relative to the vitrinitic samples A and B (Fig. 8).

Organic rich shales sampled at various depths from well 7227/8-U-3 in the neighboring Nordkapp Basin also display considerable differences in pyrolysis results relative to each other and with respect to other wells (Fig. 11C). The deepest, marine liptinite-rich sample (i.e. K), predicted to generate sulfur-rich, P–N-A low wax oils, exhibits a dominant activation energy peak at 52 kcal/mol and accordingly generates at one of the lowest temperature in the data set (Fig. 8). This sample has a relatively low HI value of 258 mg HC/g TOC given its elevated content of marine liptinites (Table 1). The E_A distribution derived for the shallower, more terrestrially influenced samples at 44m and 39.9m (i.e. J and I) shows dominant peaks in the range of 57–59 kcal/mol. These clay-rich rocks have the potential to generate intermediate, P–N-A low wax oils. Nevertheless, the sample at 44m produces a relatively higher content of sulfur-containing hydrocarbons (Fig. 5A) and starts generating at temperatures as low as those observed in the more marine, sulfur-rich sample K (Fig. 8). The elevated quantities of sulfur-bearing compounds were interpreted to result from diagenetic sulfurization of the organic matter brought about by sulfate reducing bacteria in anoxic settings. Changes in redox conditions triggered by the intermittent

Table 4
Fluid properties as a function of increasing maturity calculated from micro-scaled sealed vessels (MSSV Closed-System Pyrolysis) experiments for five selected samples.

ID	D			H			L			N			O		
	7125/1-1 (1355m)			7220/5-2 (1441m)			7229/11-1 (1260m)			7430/10-U-1 (44.1m)			7430/10-U-1 (46.95m)		
TR(%)	P_{sat} (MPa)	GOR (Sm3/Sm3)	Bo (m3/Sm3)	P_{sat} (MPa)	GOR (Sm3/Sm3)	Bo (m3/Sm3)	P_{sat} (MPa)	GOR (Sm3/Sm3)	Bo (m3/Sm3)	P_{sat} (MPa)	GOR (Sm3/Sm3)	Bo (m3/Sm3)	P_{sat} (MPa)	GOR (Sm3/Sm3)	Bo (m3/Sm3)
10	7.4	59.5	1.2	11.5	145.2	1.4	7.1	59.0	1.2	6.0	47.1	1.1	6.7	53.8	1.2
30	9.6	82.1	1.2	12.7	150.7	1.5	8.8	76.1	1.2	7.3	57.0	1.2	8.5	71.8	1.2
50	11.9	107.4	1.3	14.7	176.0	1.5	11.5	105.2	1.3	9.0	71.8	1.2	10.3	89.0	1.3
70	15.0	154.0	1.5	17.1	222.1	1.7	14.3	143.7	1.4	12.8	116.2	1.3	12.9	119.1	1.3
90	26.2	364.7	2.2	24.0	372.1	2.2	21.8	291.5	1.9	17.6	206.7	1.6	17.4	208.9	1.6

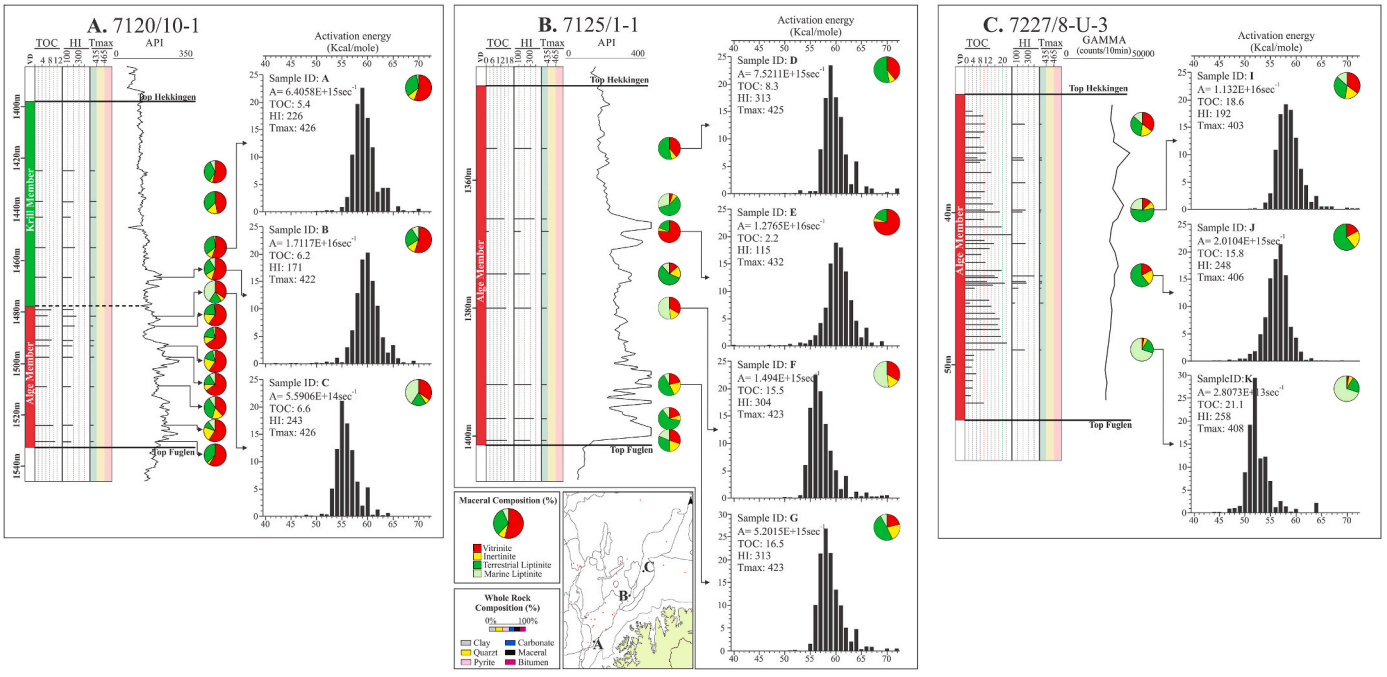

Fig. 11. Vertical variations in maceral composition and bulk kinetic parameters within the Hekkingen Formation at three different well locations: **A.** 7120/10-1 southern Hammerfest Basin; **B.** 7125/1-1 = Nysleppen Fault Complex; **C.** 7227/8-U-3 = Nordkapp Basin. TOC = total organic carbon - wt%; HI = hydrogen index – mgHC/gTOC; Tmax = Tmax Rock-Eval - °C.

growth of salt-diapirs in the Nordkapp Basin (Rojo et al., 2019; Cedeño et al., 2019) may have led to different degrees of sulfurization and hydrogen losses in the studied samples (Cedeño et al., 2021).

5.2. *Sub-regional to regional organic facies variations*

The documented variability in organic facies results from local to sub-regional geological and oceanographic controls on the sedimentation of organic-rich units across the Barents Sea (Cedeño et al., 2021). This ubiquitous heterogeneity cannot be described by bulk and quantitative pyrolysis analysis of just a few samples at different depths. Even more closely-spaced sampling intervals would only partly reproduce such variability. The current study assigns pyrolysis results from this data set to areas with comparable average maceral compositions from the subregional to regional characterization of organic facies by Cedeño et al. (2021; Fig. 2). This approach, although still uncertain, is able to more statistically and usefully reproduce changes in kinetics and petroleum type predictions. It is also important to point out that some of the pyrolyzed source rock samples in this data set come from wells drilled near structural highs (i.e. wells 7231-1-U-1, 7227/8-U-3, 7125/1-1; Fig. 2) or from well sections interpreted to have experienced substantial organic matter dilution during sedimentation (i.e. well 7120/10–1; see Fig. 4 in Cedeño et al., 2021); therefore, the generative potential in these areas may, to varying degrees, be less than that in deeper, more anoxic settings.

The maps in Fig. 12 illustrate the variations in kinetic models of bulk petroleum generation within the Alge and Krill members. The marine liptinite-rich shales of the Alge Member in the central Hammerfest Basin and their more terrestrial liptinitic equivalents to the west require the use of kinetic data derived from labile kerogen assemblages, similar to those in samples H and N (Table 2; Fig. 12A), respectively. According to the assigned parameters, the Alge Member in these marginal-to-thermally mature areas has the potential to generate intermediate, low wax P–N-A oils with overall low GOR (i.e. black oils). The high average contents of marine liptinites within both the Alge and Krill members in the Bjørnøyrenna Fault Complex, whose combined cumulative thickness exceeds 800m (Marín et al., 2020), permits the use of kinetic properties from sample H. Kinetic information from a more intermediate marine-terrestrial sample, and therefore a moderately more stable kerogen type (i.e. sample C), is assigned to the Alge source rocks in the Nysleppen Fault Complex as well as in the eastern margin of the Hammerfest Basin (Fig. 12A).

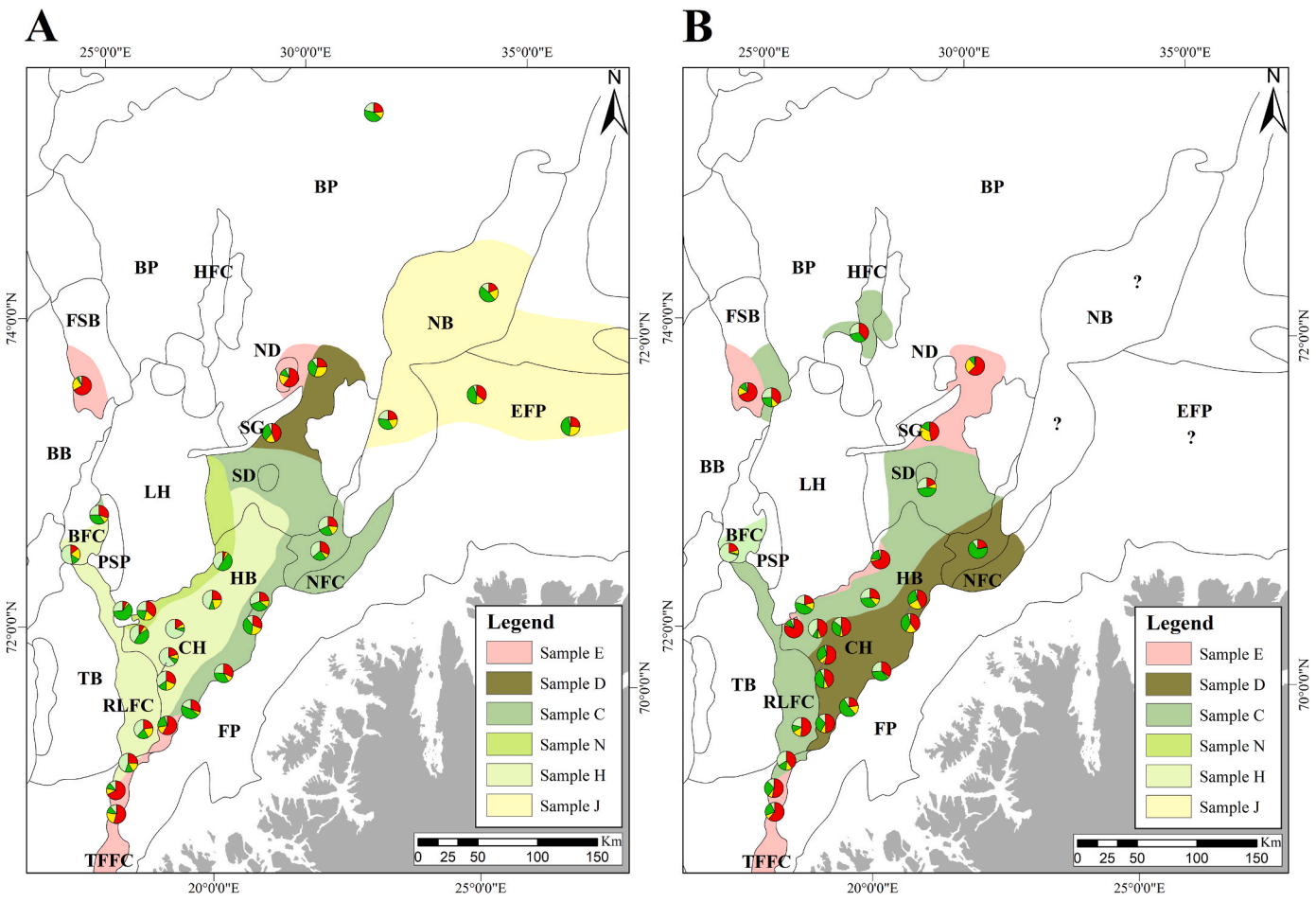

Fig. 12. Map of the southwestern Barents Sea illustrating the variability in kinetics models within the Alge (**A**) and Krill (**B**) members. Results from the current data set are assigned to areas with comparable maceral compositions from the subregional to regional characterization of organic facies by Cedeño et al., 2021.

The organic fraction within the Krill Member across most of the Hammerfest Basin consists predominantly of vitrinite and terrestrial liptinites (Fig. 12B). Thus, kinetic parameters describing the primary cracking from thermally more stable land-derived kerogens, like those in sample D, are suggested. These type III/II source rocks are expected to generate intermediate, black oils of a P–N-A low wax composition with potentially light oils generated at 90% transformation. The kinetic variability between the kerogen types assigned to the Alge and Krill members in the western-central Hammerfest Basin covers a temperature range of approximately 20 °C for the commencement of petroleum generation (Fig. 8). This shift in organic constituents within the Hammerfest Basin reflects the regional flooding that peaked during Alge times and subsequent sea level drop during Krill times.

Sources rocks of the Alge Member in the eastern Finnmark Platform feature maceral assemblages comparable to those within the Krill Member in the Hammerfest Basin (Fig. 12) and, therefore, assigning the kinetics derived from sample D seems logical. However, the pyrolysate of sample L from well 7229/11–1 in the eastern Finnmark Platform contains a high relative abundance of sulfur-bearing compounds, implying the existence, at least locally, of thermally less stable type IIS kerogens. Although both D and L samples have the potential to generate low wax P–N-A, black oils, the onset of generation in sample L takes place approximately 17 °C earlier than in sample D (Fig. 8), challenging the use of either set of kinetics. Additionally, it is possible that the sulfur content, and so the thermal stability, varies throughout the section as was the case in well 7227/8-U-3 from the Nordkapp Basin. This study provisionally assigns kinetics parameters from an organically comparable source rock sample with a sulfur content that is intermediate between sample L and D, that is, sample J.

The kerogen in both the Alge and Krill members within the Fingerdjupet Sub-basin and the Troms-Finnmark Fault Complex is composed mostly of hydrogen-poor vitrinitic macerals, which are at best only gas & condensate prone. In this case, kinetic parameters characteristic of the thermally very stable vitrinitic kerogen in sample E are suitable. Gas and condensate prone source rocks also occur within both members at some localities along the Hammerfest Basin-Loppa High boundary.

6. Conclusions

The investigated organic rich samples from the Hekkingen Formation contain varying proportions of kerogen type II and III, as demonstrated by their hydrogen richness and maceral assemblages. Heterogeneities in the kerogen composition result in different orders of kinetic stability, with the predicted onset of petroleum generation spread over a relatively high and wide temperature range from 123 °C to 144 °C (at 3.3C°/Ma). This temperature range equates to a difference of up to 700 m of burial if a thermal gradient of 30 °C is assumed.

With a few exceptions, the variability in activation energy distributions, and so in kerogen thermal stability, results from variations in the kerogen maceral composition. Marine liptinite-rich samples show a low and narrow range of activation energies relative to the higher and broader range described for the more terrestrial samples. Reduced kerogen stability associated with elevated sulfur contents is documented in a few samples.

The majority of the investigated samples have the potential to generate low GOR oils of an intermediate to aromatic, low wax P–N-A

composition along with variable amounts of wet gas in the range of 25–35%. Petroleum of similar compositional and physical properties is predicted to have been generated from the natural maturation series of various organic facies in mature areas of the Hammerfest Basin, the Ringvassøy-Loppa High and the Bjørnøyrenna fault complexes.

Upon maturation, it is likely that discreet intervals in the Nordkapp Basin and eastern Finnmark Platform may generate high-sulfur, low wax P–N-A oils with low GOR. Vitrinite-rich sources in the Fingerdjupet Sub-basin and the Troms-Finnmark Fault Complex have a potential for gas and condensate generation at late maturities.

Declaration of competing interest

The authors declare that they have no known competing financial interests or personal relationships that could have appeared to influence the work reported in this paper.

Acknowledgments

The authors would like to thank the sponsors of the JuLoCrA project (https://wp.ux.uis.no/julocra/) for providing essential economic support. We are grateful to Integrated Geochemical Interpretation (IGI) for free software supply and to Applied Petroleum Technologies (APT) for analytical studies, particularly to Per Erling Johansen. The authors also thank reviewers Simon George and Dag Arild Karlsen for their constructive reviews that greatly improved the manuscript.

References

Abay, T.B., Karlsen, D.A., Pedersen, J.H., Olaussen, S., Backer-Owe, K., 2017. Thermal maturity, hydrocarbon potential and kerogen type of some Triassic-Lower Cretaceous sediments from the SW Barents Sea and Svalbard. Petrol. Geosci. 24, 349–373. https://doi.org/10.1144/petgeo2017-035.

Århus, N., 1991. The transition from deposition of condensed carbonates to dark claystones in the Lower Cretaceous succession of the southwestern Barents Sea. Nor. Geol. Tidsskr. 71, 259–263.

Berglund, L., Augustson, J., Færseth, R., Gjelberg, J., Ramberg-Moe, H., 1986. The evolution of the Hammerfest Basin. Habitat of hydrocarbons on the Norwegian continental shelf. Norsk Petroleumsforening 319–338.

Blaich, O.A., Tsikalas, F., Faleide, J.I., 2017. New insights into the tectono-stratigraphic evolution of the southern stappen high and its transition to Bjørnøya Basin, SW Barents Sea. Mar. Petrol. Geol. 85, 89–105. https://doi.org/10.1016/j.marpetgeo.2017.04.015.

Braun, R.L., Burnham, A.K., Reynolds, J.G., Clarkson, J.E., 1991. Pyrolysis kinetics for lacustrine and marine source rocks by programmed micropyrolysis. Energy Fuel. 5, 192–204. https://doi.org/10.1021/ef00025a033.

Bugge, T., Elvebakk, G., Fanavoll, S., Mangerud, G., Smelror, M., Weiss, H.M., Gjelberg, J., Kristensen, S.E., Nilsen, K., 2002. Shallow stratigraphic drilling applied in hydrocarbon exploration of the Nordkapp Basin, Barents Sea. Mar. Petrol. Geol. 19, 13–37. https://doi.org/10.1016/S0264-8172(01)00051-4.

Burnham, A.K., Braun, R.L., Gregg, H.R., Samoun, A.M., 1987. Comparison of methods for measuring kerogen pyrolysis rates and fitting kinetic parameters. Energy Fuel. 1, 452–458. https://doi.org/10.1021/ef00006a001.

Castelli, A., Chiaramonte, M.A., Beltrame, P.L., Carniti, P., Del Bianco, A., Stroppa, F., 1990. Thermal degradation of kerogen by hydrous pyrolysis. A kinetic study. Org. Geochem. 16, 75–82. https://doi.org/10.1016/0146-6380(90)90027-W.

Cavanagh, A.J., Di Primio, R., Scheck-Wenderoth, M., Horsfield, B., 2006. Severity and timing of cenozoic exhumation in the southwestern Barents Sea. J. Geol. Soc. 163, 761–774. https://doi.org/10.1144/0016-76492005-146.

Cedeño, A., Rojo, L.A., Cardozo, N., Centeno, L., Escalona, A., 2019. The impact of salt tectonics on the thermal evolution and the petroleum system of confined rift basins: insights from basin modeling of the Nordkapp Basin, Norwegian Barents Sea. Geosciences 9. https://doi.org/10.3390/geosciences9070316.

Cedeño, A., Ohm, S., Escalona, A., Marín, D., Olaussen, S., Demchuck, T., 2021. Upper Jurassic to Lower Cretaceous Source Rocks in the Norwegian Barents Sea, Part I: Organic Geochemical, Petrographic, and Paleogeographic Investigations.

Clark, S., Glorstad-Clark, E., Faleide, J., Schmid, D., Hartz, E., Fjeldskaar, W., 2014. Southwest Barents Sea rift basin evolution: comparing results from backstripping and time-forward modelling. Basin Res. 26, 550–566. https://doi.org/10.1111/bre.12039.

Cornford, C., 1998. Source rocks and hydrocarbons of the north sea. In: Glennie, K.W. (Ed.), Petroleum Geology of the North Sea. Blackwell Science, Oxford, pp. 376–462. https://doi.org/10.1002/9781444313413.ch11.

Dalland, A., Worsley, D., Ofstad, K., 1988. A lithostratigraphic scheme for the Mesozoic and Cenozoic succession offshore Norway north of 62 N. Norwegian Petroleum Directorate Bulletin 4, 67.

Demaison, G.J., Moore, G.T., 1980. Anoxic environments and oil source bed genesis. AAPG (Am. Assoc. Pet. Geol.) Bull. 64, 1179–1209. https://doi.org/10.1306/2F91945E-16CE-11D7-8645000102C1865D.

di Primio, R., Horsfield, B., 1996. Predicting the generation of heavy oils in carbonate/evaporitic environments using pyrolysis methods. Org. Geochem. 24, 999–1016. https://doi.org/10.1016/S0146-6380(96)00116-7.

di Primio, R., Horsfield, B., 2006. From petroleum-type organofacies to hydrocarbon phase prediction. AAPG (Am. Assoc. Pet. Geol.) Bull. 90, 1031–1058. https://doi.org/10.1306/02140605129.

di Primio, R., Skeie, J.E., 2004. Development of a compositional kinetic model for hydrocarbon generation and phase equilibria modelling: a case study from Snorre field, Norwegian North Sea. In: Cubitt, J.M., England, W.A., Larter, S.R. (Eds.), Understanding Petroleum Reservoirs: towards an Integrated Reservoir Engineering and Geochemical Approach, vol. 237. Geological Society (London) Special Publication, pp. 157–174.

di Primio, R., Dieckmann, V., Mills, N., 1998. PVT and phase behavior analysis in petroleum exploration. Org. Geochem. 29, 207–222. https://doi.org/10.1016/S0146-6380(98)00102-8.

Dieckmann, V., Keym, M., 2006. A new approach to bridge the effect of organofacies variations on kinetic modelling and geological extrapolations. Org. Geochem. 37, 728–739. https://doi.org/10.1016/j.orggeochem.2005.12.008.

Dieckmann, V., Schenk, H.J., Horsfield, B., Welte, D.H., 1998. Kinetics of petroleum generation and cracking by programmed-temperature closed-system pyrolysis of Toarcian Shales. Fuel 77, 23–31. https://doi.org/10.1016/S0016-2361(97)00165-8.

Doré, A.G., Scotchman, I.C., Corcoran, D., 2000. Cenozoic exhumation and prediction of the hydrocarbon system on the NW European margin. J. Geochem. Explor. 69–70, 615–618. https://doi.org/10.1016/S0375-6742(00)00137-0.

Duran, E.R., di Primio, R., Anka, Z., Stoddart, D., Horsfield, B., 2013a. Petroleum system analysis of the Hammerfest Basin (southwestern Barents Sea): comparison of basin modelling and geochemical data. Org. Geochem. 63, 105–121. https://doi.org/10.1016/j.orggeochem.2013.07.011.

Duran, E.R., di Primio, R., Anka, Z., Stoddart, D., Horsfield, B., 2013b. 3D-basin modelling of the Hammerfest Basin (southwestern Barents Sea): a quantitative assessment of petroleum generation, migration, and leakage. Mar. Petrol. Geol. 45, 281–303. https://doi.org/10.1016/j.marpetgeo.2013.04.023.

Eglinton, T.I., Sinninghe Damsté, J.S., Kohnen, M.E.L., de Leeuw, J.W., Larter, S.R., Patience, R.L., 1990. Analysis of maturity-related changes in the organic sulfur composition of kerogens by flash pyrolysis–gas chromatography. In: Geochemistry of Sulfur in Fossil Fuels. American Chemical Society, pp. 529–565. https://doi.org/10.1021/bk-1990-0429.ch027.

Eglinton, T.I., Sinninghe Damsté, J.S., Pool, W., de Leeuw, J.W., Eijk, G., Boon, J.J., 1992. Organic sulphur in macromolecular sedimentary organic matter. II. Analysis of distributions of sulphur-containing pyrolysis products using multivariate techniques. Geochem. Cosmochim. Acta 56, 1545–1560. https://doi.org/10.1016/0016-7037(92)90224-7.

Faleide, J.I., Vågnes, E., Gudlaugsson, S.T., 1993. Late Mesozoic-Cenozoic evolution of the south-western Barents Sea in a regional rift-shear tectonic setting. Mar. Petrol. Geol. 10, 186–214. https://doi.org/10.1016/0264-8172(93)90104-Z.

Espitalié, J., Madec, M., Tissot, B.P., Menning, J.J., Leplat, P., 1977. Source Rock Characterization Method for Petroleum Exploration. Institut Francais du Petrole, Labofina, SA.

Faleide, T.S., Midtkandal, I., Planke, S., Corseri, R., Faleide, J.I., Serck, C.S., Nystuen, J. P., 2019. Characterization and development of Early Cretaceous shelf platform deposition and faulting in the Hoop area, southwestern Barents Sea-constrained by high-resolution seismic data. Norw. J. Geol. 99, 3. https://doi.org/10.17850/njg99-3-7.

Georgiev, S.V., Stein, H.J., Hannah, J.L., Xu, G.P., Bingen, B., Weiss, H.M., 2017. Timing, duration, and causes for late jurassic-early cretaceous anoxia in the Barents Sea. Earth Planet Sci. Lett. 461, 151–162. https://doi.org/10.1016/j.epsl.2016.12.035.

Gernigon, L., Brönner, M., Roberts, D., Olesen, O., Nasuti, A., Yamasaki, T., 2014. Crustal and basin evolution of the southwestern Barents Sea: from Caledonian orogeny to continental breakup. Tectonics 33, 347–373. https://doi.org/10.1002/2013TC003439.

Hartwig, A., di Primio, R., Anka, Z., Horsfield, B., 2012. Source rock characteristics and compositional kinetic models of Cretaceous organic rich black shales offshore southwestern Africa. Org. Geochem. 51, 17–34. https://doi.org/10.1016/j.orggeochem.2012.07.008.

Helleren, S., Marín, D., Ohm, S., Augustsson, C., Escalona, A., 2020. Why does not lithology correlate with gamma-ray spikes in the shaley source rocks of the Upper Jurassic Alge Member (southwestern Barents Sea)? Mar. Petrol. Geol. 121 https://doi.org/10.1016/j.marpetgeo.2020.104623.

Henriksen, E., Ryseth, A., Larssen, G., Heide, T., Rønning, K., Sollid, K., Stoupakova, A., 2011a. Tectonostratigraphy of the greater Barents Sea: implications for petroleum systems. In: Spencer, A.M., Embry, A.F., Gautier, D.L., Stoupakova, A.V., Sørensen, K. (Eds.), Arctic Petroleum Geology, vol. 35. Geological Society, London, pp. 163–195. https://doi.org/10.1144/M35.10. Memoirs 2011.

Henriksen, E., Bjørnseth, H.M., Hals, T.K., Heide, T., Kiryukhina, T., Kløvjan, O.S., Larssen, G.B., 2011b. Uplift and erosion of the greater Barents Sea: impact on prospectivity and petroleum systems. In: Spencer, A.M., Embry, A.F., Gautier, D.L., Stoupakova, A.V., Sørensen, K. (Eds.), Arctic Petroleum Geology, vol. 35. Geological Society, London, pp. 271–281. https://doi.org/10.1144/M35.17. Memoirs 2011.

Horsfield, B., 1997. The bulk composition of first-formed petroleum in source rocks. In: Welte, D.H., Horsfield, B., Baker, D.R. (Eds.), Petroleum and Basin Evolution. Springer Verlag, Berlin, Heidelberg, pp. 337–402.

Horsfield, B., Disko, U., Leistner, F., 1989. The micro-scale simulation of maturation: outline of a new technique and its potential applications. Geol. Rundsch. 78, 361–374.
Horsfield, B., Schenk, H.J., Mills, N., Welte, D.H., 1992. An investigation of the inreservoir conversion of oil to gas: compositional and kinetic findings from closed-system programmed-temperature pyrolysis. Org. Geochem. 19, 191–204. https://doi.org/10.1016/0146-6380(92)90036-W.
Indrevær, K., Gabrielsen, R.H., Faleide, J.I., 2017. Early Cretaceous synrift uplift and tectonic inversion in the Loppa High area, southwestern Barents Sea, Norwegian shelf. J. Geol. Soc. 174, 242–254. https://doi.org/10.1144/jgs2016-066.
Kairanov, B., Marín, D., Escalona, A., Cardozo, N., 2019. Growth and linkage of a Basin-bounding fault system: insights from the early cretaceous evolution of the northern Polhem subplatform, SW Barents Sea. J. Struct. Geol. 124, 182–196. https://doi.org/10.1016/j.jsg.2019.04.014.
Kairanov, B., Escalona, A., Norton, I., Abrahamsson, P., 2021. Early cretaceous evolution of the Tromsø Basin, SW Barents Sea. Mar. Petrol. Geol. 123 https://doi.org/10.1016/j.marpetgeo.2020.104714.
Kaplan, I.R., Emery, K.O., Rittenbebg, S.C., 1963. The distribution and isotopic abundance of sulphur in recent marine sediments off southern California. Geochem. Cosmochim. Acta 27, 313–331. https://doi.org/10.1016/0016-7037(63)90074-7.
Karlsen, D.A., Larter, S.R., 1991. Analysis of petroleum fractions by TLC-FID: applications to petroleum reservoir description. Org. Geochem. 17 (5), 603–617. https://doi.org/10.1016/0146-6380(91)90004-4.
Killops, S., Stoddart, D., Mills, N., 2014. Inferences for sources of oils from the Norwegian Barents Sea using statistical analysis of biomarkers. Org. Geochem. 76, 157–166. https://doi.org/10.1016/j.orggeochem.2014.07.011.
Larter, S.R., Horsfield, B., 1993. Determination of structural components of kerogens by the use of analytical pyrolysis methods. In: Engel, M.H., Macko, S.A. (Eds.), Organic Geochemistry. Plenum Press, New York, pp. 271–287.
Lerch, B., Karlse, D.A., Matapour, Z., Seland, R., Backer-Owe, K., 2016. Organic geochemistry of Barents Sea petroleum: thermal maturity and alteration and mixing processes in oils and condensates. J. Petrol. Geol. 39, 125–147. https://doi.org/10.1111/jpg.12637.
Mango, F.D., 1996. Transition metal catalysis in the generation of natural gas. Org. Geochem. 24, 977–984. https://doi.org/10.1016/0016-7037(92)90153-A.
Mango, F.D., 2000. The origin of light hydrocarbons. Geochem. Cosmochim. Acta 64, 1265–1277. https://doi.org/10.1016/0016-7037(90)90156-F.
Mango, F.D., 2001. Methane concentrations in natural gas: the genetic implications. Org. Geochem. 32, 1283–1287. https://doi.org/10.1016/S0146-6380(01)00099-7.
Marín, D., Escalona, A., Grundvåg, S.A., Olaussen, S., Sandvik, S., Śliwińska, K.K., 2018. Unravelling key controls on the rift climax to post-rift fill of marine rift basins: insights from 3D seismic analysis of the Lower Cretaceous of the Hammerfest Basin, SW Barents Sea. Basin Res. 30, 587–612. https://doi.org/10.1111/bre.12266.
Marín, D., Helleren, S., Escalona, A., Olaussen, S., Cedeño, A., Nøhr-Hansen, H., Ohm, S., 2020. The Middle Jurassic to lowermost Cretaceous in the SW Barents Sea: interplay between tectonics, coarse-grained sediment supply and organic matter preservation. Basin Res. https://doi.org/10.1111/bre.12504.
Mørk, A., Dallmann, W., Dypvik, H., Johannessen, E., Larssen, G., Nagy, J., Nøttvedt, A., Olaussen, S., Pchelina, T., Worsley, D., 1999. Mesozoic Lithostratigraphy. Lithostratigraphic Lexicon of Svalbard. Upper Paleozoic to Quaternary Bedrock. Review and Recommendations for Nomenclature Use, pp. 127–214.
Mulrooney, M.J., Leutscher, J., Braathen, A., 2017. A 3D structural analysis of the Goliat field, Barents Sea, Norway. Mar. Petrol. Geol. 86, 192–212. https://doi.org/10.1016/j.marpetgeo.2017.05.038.
Murillo, W.A., Vieth-Hillebrand, A., Horsfield, B., Wilkes, H., 2016. Petroleum source, maturity, alteration and mixing in the southwestern Barents Sea: new insights from geochemical and isotope data. Mar. Petrol. Geol. 70, 119–143. https://doi.org/10.1016/j.marpetgeo.2015.11.009.
Ohm, S.E., Karlsen, D.A., Austin, T., 2008. Geochemically driven exploration models in uplifted areas: examples from the Norwegian Barents Sea. AAPG (Am. Assoc. Pet. Geol.) Bull. 92, 1191–1223. https://doi.org/10.1306/06180808028.
Orr, W.L., 1986. Kerogen/asphaltene/sulfur relationships in sulfur-rich Monterey oils. Org. Geochem. 10, 499–516. https://doi.org/10.1016/0146-6380(86)90049-5.
Pedersen, K.S., Thomassen, P., Fredenslund, A., 1985. Thermodynamics of petroleum mixtures containing heavy hydrocarbons. 3. Efficient flash calculation procedures using the SRK equation of state. Ind. Eng. Chem. Process Des. Dev. 24, 948–954. https://doi.org/10.1021/i200031a009.
Petersen, H., Rosenberg, P., 2000. The relationship between the composition and rank of humic coals and their activation energy distributions for the generation of bulk petroleum. Petrol. Geosci. 6, 137–149. https://doi.org/10.1144/petgeo.6.2.137.
Reynolds, J.G., Burnham, A.K., 1995. Comparison of kinetic analysis of source rocksand kerogen concentrates. Org. Geochem. 23, 11–19. https://doi.org/10.1016/0146-6380(94)00114-G.
Riis, F., 1996. Quantification of Cenozoic vertical movements of Scandinavia by correlation of morphological surfaces with offshore data. Global Planet. Change 331–357. https://doi.org/10.1016/0921-8181(95)00027-5.
Rojo, L.A., Cardozo, N., Escalona, A., Koyi, H., 2019. Structural style and evolution of the Nordkapp Basin, Norwegian Barents Sea. AAPG (Am. Assoc. Pet. Geol.) Bull. 103 (9), 2177–2217. https://doi.org/10.1306/01301918028.
Santamaria Orozco, D.M., 2000. Organic geochemistry of tithonian source rocks and associated oils from the sonda de Campeche. Forschungszentrum Jülich GmbH Zentralbibliothek. Verlag Jülich, p. 201.
Schaeffer, P., Reiss, C., Albrecht, P., 1995. Geochemical study of macromolecular organic matter from sulfur-rich sediments of evaporitic origin (Messinian of Sicily) by chemical degradations. Org. Geochem. 23, 567–581. https://doi.org/10.1016/0146-6380(95)00045-G.
Schenk, H.J., Horsfield, B., Krooss, B., Schaefer, R.G., Schwochau, K., 1997. Kinetics of petroleum formation and cracking. In: Welte, D.H., Horsfield, B., Baker, D.R. (Eds.), Petroleum and Basin Evolution. Springer-Verlag, Berlin Heidelberg, pp. 231–270.
Scotese, C.R., 2016. PALEOMAP PaleoAtlas for GPlates and the PaleoData Plotter Program. PALEOMAP Project. http://www.earthbyte.org/paleomap-paleoatlas-for-gplates/.
Serck, C.S., Faleide, J.I., Braathen, A., Kjølhamar, B., Escalona, A., 2017. Jurassic to early cretaceous basin configuration(s) in the Fingerdjupet subbasin, SW Barents Sea. Mar. Petrol. Geol. 86, 874–891. https://doi.org/10.1016/j.marpetgeo.2017.06.044.
Sinninghe Damste, J.S., Eglington, T.I., de Leeuw, J.W., Schenck, P.A., 1989. Organic sulphur in macromolecular sedimentary organic matter: I. Structure and origin of sulphur-containing moieties in kerogen, asphaltenes and coal as revealed by flash pyrolysis. Geochem. Cosmochim. Acta 53, 873–889. https://doi.org/10.1016/0016-7037(89)90032-X.
Smelror, M., Mørk, A., Mørk, M.B.E., Weiss, H.M., Løseth, H., 2001. Middle Jurassic-Lower Cretaceous transgressive-regressive sequences and facies distribution off northern Nordland and Troms, Norway, 10. Norwegian Petroleum Society Special Publications, pp. 211–232. https://doi.org/10.1016/S0928-8937(01)80015-1.
Sund, T., Skarpnes, O., Jensen, L.N., Larsen, R.M., 1986. Tectonic development and hydrocarbon potential offshore Troms, northern Norway. In: Halbouty, T.H. (Ed.), Future Petroleum Provinces of the World, vol. 40. AAPG Memoir. https://doi.org/10.1306/M40454C29.
Tegelaar, E.W., Noble, R.A., 1994. Kinetics of hydrocarbon generation as a function of the molecular structure of kerogen as revealed by pyrolysis–gas chromatography. Org. Geochem. 22, 543–574. https://doi.org/10.1016/0146-6380(94)90125-2.
Tegelaar, E.W., de Leeuw, J.W., Derenne, S., Largeau, C., 1989. A reappraisal of kerogen formation. Geochem. Cosmochim. Acta 53, 3103–3106. https://doi.org/10.1016/0016-7037(89)90191-9.
Tissot, B.P., Welte, D.H., 1984. Petroleum Formation and Occurrence. Springer Verlag, Berlin.
Tissot, B.P., Pelet, R., Ungerer, P., 1987. Thermal history of sedimentary basins, maturation indices, and kinetics of oil and gas generation. AAPG (Am. Assoc. Pet. Geol.) Bull. 71, 1445–1466. https://doi.org/10.1306/703C80E7-1707-11D7-8645000102C1865D.
Tsikalas, F., Blaich, O.A., Faleide, J.I., Olaussen, S., 2021. Stappen High-Bjørnøya Tectono-Sedimentary Element, Barents Sea, vol. 57. Geological Society, London, Memoirs. https://doi.org/10.1144/M57-2016-24.
Urov, K.E., 1980. Thermal decomposition of kerogens: mechanism and analytical application. J. Anal. Appl. Pyrol. 1, 323–338. https://doi.org/10.1016/0165-2370(80)80016-7.
Van Dongen, B.E., Schouten, S., Baas, M., Geenevasen, J.A.J., Sinninghe Damste, J.S., 2003. An Experimental Study of the Low-Temperature Sulfurization of Carbohydrates. https://doi.org/10.1016/S0146-6380(03)00060-3.
Wierzbowski, A., Smelror, M., 2020. The bajocian to kimmeridgian (Middle to upper jurassic) ammonite succession at sentralbanken high (core 7533/3-U-1), Barents Sea, and its stratigraphical and palaeobiogeographical significance. Volumina Jurassica 18, 1–22. https://doi.org/10.7306/vj.18.1.
Zabinsky, Z.B., 1998. Stochastic methods for practical global optimization. J. Global Optim. 13, 433–444.
Zabinsky, Z.B., Smith, R.L., McDonald, J.F., Romeijn, H.E., Kaufman, D.E., 1993. Improving hit and run for global optimization. J. Global Optim. 3, 171–192.